N-MP: A network-state-based Max Pressure algorithm incorporating regional perimeter control

Hao Liu[a,*], Vikash V. Gayah[a]

[a] *The Pennsylvania State University, University Park, PA, United States*

Abstract

The Max Pressure (MP) framework has been shown to be an effective real-time decentralized traffic signal control algorithm. However, despite its superior performance and desirable features – such as the maximum stability property – it may still suffer from deterioration in network mobility due to the rise of congestion within specific regions of an urban traffic network. To address this drawback and further improve the performance of MP control in urban networks, this paper proposes a novel MP algorithm that incorporates regional traffic states into the MP framework. The proposed model – called N-MP – simultaneously integrates perimeter metering control at the boundary of regions of a network to be protected with traditional local intersection control. The proposed model is the first to incorporate perimeter metering control fully within a decentralized signal control environment and inherits the maximum stability property. In addition, it does not require extra traffic state measurements compared to the original MP algorithms, beyond a measure of congestion within the protected region of the network. Microscopic traffic simulation results demonstrate that the proposed model can outperform two baseline perimeter control models – bang-bang control and feedback gating – under various traffic conditions. More interestingly, this superiority is maintained in both fully and partially connected environments.

Keywords: Max Pressure; Perimeter control; Decentralized traffic signal control; Macroscopic Fundamental Diagram; Connected vehicles

1. Introduction

Traffic signal timing plays a key role in the operational performance of urban transportation networks. Compared to fixed-time and actuated control strategies, adaptive signal control can enhance operational efficiency by adjusting signal timings in real-time based on the prevailing traffic conditions. Numerous adaptive traffic signal control methods have been developed. Adaptive signal control methods can be categorized as centralized and decentralized control approaches, based on the architecture of communication between controllers and traffic environment. The former requires communication and coordination between individual intersections and makes signal timing decisions jointly for all signals, while each intersection operates independently in the latter. Well-known centralized control methods include SCOOT (Hunt et al., 1981), OPAC (Gartner, 1983), SCATS (Lowrie, 1990), UTOPIA (Mauro and Di Taranto, 1990) and RHODES (Mirchandani and Head, 2001). In general, the computational complexity for these methods increases exponentially with the network size, which is a significant bottleneck for implementation. On the contrary, the computational burden required by the decentralized control methods is linear to the network size. Therefore, decentralized control methods are the more attractive strategy for large networks. Thanks to this advantage in computational efficiency, recent research efforts have shifted to decentralized signal control algorithms.

*Corresponding author

Email addresses: hfl5376@psu.edu (Hao Liu), gayah@engr.psu.edu (Vikash V. Gayah)

1.1. Max Pressure signal control methods

Max Pressure (MP) has become a very popular real-time decentralized traffic signal control algorithm. It was initially proposed to tackle the packet scheduling issue in wireless communication networks (Tassiulas and Ephremides, 1990), but later applied to traffic signal control by Varaiya (2013). Under MP control, signal timings at an intersection are determined based on the *pressure* of individual signal phases, which are obtained using local traffic states as input. In addition to computational efficiency, other favorable properties of MP algorithms include: (1) no requirement of demand information/estimation; and, (2) the *maximum stability* property. The latter theoretically proves that MP can serve any demand that can be served by a feasible control policy. Many MP variants (Levin et al., 2020; Le et al., 2015; Xiao et al., 2014; Gregoire et al., 2014; Mercader et al., 2020; Wu et al., 2017; Dixit et al., 2020; Liu and Gayah, 2022, 2023; Xu et al., 2022; Wang et al., 2022; Li and Jabari, 2019) have been proposed in the past decade. A comprehensive review of MP-based traffic signal control algorithms can be found in (Levin, 2023).

The performance of an MP algorithm highly depends on the metric used to compute the pressure of each phase. Varaiya (2013) used the number of vehicles on both upstream and downstream links as the proposed metric; however, this metric does not consider the moving status of vehicles and the impact of vehicle storage capacity. Both of these factors can affect the control performance significantly. Various modifications have been proposed to address these issues. Gregoire et al. (2014) proposed a model that explicitly considers the queue capacity of links. Li and Jabari (2019) developed a position-weighted backpressure (PWBP) that incorporates the relative position of vehicles on the link. Wang et al. (2022) developed a model to consider the influence of lost time between phase changes. In addition to the number of vehicles, travel time-based (Mercader et al., 2020) and travel delay-based (Dixit et al., 2020; Liu and Gayah, 2022, 2023) MP algorithms have also been developed.

Despite their favorable performance and architecture, MP algorithms still have space for improvements. One drawback is that the control action is purely based on current local traffic states and does not consider its impact on the operational efficiency at a regional level. One consequence of this feature is that MP cannot prevent oversaturation, nor can it maintain operating efficiency of a region under excessive external demand, which is referred to as a protected region. Such a case is common for urban transportation networks; e.g., a dense downtown region surrounded by a less dense suburb during the morning commute. On the contrary, MP algorithms activate the phase to release the pressure from the movements with the largest pressure; e.g., the movements with the longest queue length or highest delay. This may result in sending more vehicles intoto the busy region, which could exacerbate regional congestion.

1.2. Perimeter control strategy

One way to prevent congestion in busy protected regions is perimeter control (PC), which has been derived based on the notion of network Macroscopic Fundamental Diagram (MFD). A well-defined MFD conveys an unimodal relationship between the use (e.g., vehicle density or accumulation) and productivity (e.g., average flow or trip completion rate) aggregated across a network. The existence of an MFD was first posited by Godfrey (1969) and later demonstrated in both theoretical (Daganzo, 2007) and empirical (Geroliminis and Daganzo, 2008) studies.

Although the actual shape of an MFD depends on various factors – including network structure (Ortigosa and Menendez, 2014; Knoop et al., 2014; Xu and Gayah, 2023), signal timings (Zhang et al., 2013; Alonso et al., 2019), vehicle routing (Gayah and Daganzo, 2011; Xu et al., 2020), etc. – a critical density always exists on an MFD at which the network productivity is maximized. The network falls into the congestion domain once the average density exceeds this critical value. To maintain the efficiency of a protected region during busy hours, PC tries to keep the region near the critical density by metering or limiting the inflows into the region via intersections on the periphery of the protected region, referred to as perimeter intersections. Various PC algorithms have been developed, such as bang-bang control (Daganzo, 2007), proportion-integral-type (PI) feedback control (Keyvan-Ekbatani et al., 2012; Ramezani et al., 2015; Haddad and Shraiber, 2014) and reinforcement learning-based approaches (Ni and Cassidy, 2019; Zhou and Gayah, 2021, 2023). A common way to implement PC is to adjust the signal timings at the perimeter intersections to reduce the green time for inbound movements, i.e., those approaches sending vehicles into the protected

region. The performance of PC has been demonstrated by numerous studies (Daganzo, 2007; Keyvan-Ekbatani et al., 2012; Ramezani et al., 2015; Haddad and Shraiber, 2014; Ni and Cassidy, 2019; Zhang et al., 2020), and a review for perimeter control approaches can be found in (Zhang et al., 2020).

1.3. Proposed network-state-based MP algorithm

Inspired by PC strategies, this paper proposes a network-state-based MP algorithm, referred to as N-MP, that incorporates regional traffic conditions in the protected region into the MP architecture. Doing so facilitates the application of perimeter metering control *within* the MP framework while maintaining the regional operating efficiency under heavy external demand scenarios. Specifically, N-MP considers a reduction in the pressure calculation for all phases serving inbound movements at the perimeter intersections when the average density in the protected region exceeds the critical value. This in turn reduces the green time for inbound movements, so the inflows can be effectively restricted. Like PC algorithms, N-MP can be implemented at the periphery of the protected region. The delay-based MP algorithm proposed in (Liu and Gayah, 2022), called D-MP, uses travel delay as the metric for pressure calculation and has been demonstrated to outperform the number of vehicle-based and travel time-based MP algorithms under various traffic conditions. Therefore, we use D-MP as the building block for the development of N-MP. However, the mechanism behind N-MP is not limited by the metric selected; i.e., this mechanism can be applied to MP algorithms based on other metrics and is expected to achieve similar improvement in the network efficiency as the proposed N-MP.

To the best of our knowledge, this is the first work to incorporate regional perimeter control directly within the MP algorithm framework. To the authors' knowledge, Tsitsokas et al. (2023) and Su et al. (2023) are the only related works that combine PC and MP control; however, both studies separately implement MP algorithms at non-perimeter intersections and non-MP-based PC algorithms at perimeter intersections to limit inflows to the protected region responding to the occurrence of congestion. (Tsitsokas et al., 2023) implemented the PI feedback control (Keyvan-Ekbatani et al., 2012) at perimeter intersections while (Su et al., 2023) developed a reinforcement learning algorithm for PC. Although the joint implementation can improve the network mobility, in both works, the MP control and PC operate independently. Additionally, the PI feedback control requires additional models to determine the gated flows and the corresponding green time allocation across all perimeter intersections, and the reinforcement learning sets the same proportion of green time to all movements sending vehicles to the protected region, i.e., the algorithm imposes the same restriction across the boundary of the protected region, which can lead to questionable control performance when the protected region is heterogeneous, which is the typical pattern for congested networks. On the contrary, N-MP serves as a PC strategy *within* the MP structure. Since MP determines signal timings solely based on the pressure of the phases, it does not require extra models. In addition, a clustered N-MP is proposed to tackle traffic congestion heterogeneity of the protected region.

The contributions of the proposed model are three-fold: (1) this is the first work to incorporate regional perimeter control within the MP control architecture without the need for extra traffic states compared to the purely MP-controlled framework (other than knowledge of congestion level in the protected region); (2) the proposed strategy inherits the maximum stability property, which is the most desirable property of MP algorithms; and, (3) the proposed mechanism is transferable to MP algorithms using different types of metrics, such as number of vehicles, travel time and travel delay.

1.4. Organization

The remainder of the paper is organized as follows. Section 2 derives the N-MP algorithm and provides the proof of the maximum stability property. Section 3 demonstrates that the proposed algorithms can outperform two baseline PC models under various traffic conditions including partially connected environment. Section 4 summarizes the work and proposes future research directions.

2. Methodology

The used notations are summarized in Table 1 to help readers better follow equations in the rest of this paper.

Table 1: Description of variables

Network components and signal configuration	
$\mathcal{N}$	Set of intersections
$\mathcal{L}$	Set of links
$\mathcal{L}_{\text{enter}}$	Set of entry links
$\mathcal{L}_{\text{exit}}$	Set of exit links
$\mathcal{L}_{\text{internal}}$	Set of internal links
$\mathcal{IN}_l$	Set of incoming links of link l
$\mathcal{OUT}_l$	Set of outgoing links of link l
(l, m)	Vehicle movement defined as a pair of incoming link $l \in \mathcal{L}$ and outgoing link $m \in \mathcal{L}$ at the same intersection
$\mathcal{M}^i$	Set of movements at intersection i
$\mathcal{M}^p$	Set of the inbound movements sending vehicles into the busy (protected) region
$\mathcal{S}^i$	Set of signal phases at intersection i
S^{ij}	The jth signal phase at intersection i, which is a vector in which every element is a binary variable indicating whether the associated movement is served by this phase
Traffic dynamics	
$x^s_{l,m}(t)$	Number of stopped vehicles on movement (l, m) at time t
$x^m_{l,m}(t)$	Number of moving vehicles on movement (l, m) at time t
$x^{m\to s}_{l,m}(t)$	Number of moving vehicles at time $t-1$ that join stopped vehicles at time t on movement (l, m)
$x^{s\to \text{dis}}_{l,m}(t)$	Number of stopped vehicles on movement (l, m) at time $t-1$ that are going to depart at time t
$x^{total\to dis}_{l,m}(t)$	Total number of vehicles that will leave movement (l, m) at time t
$Q_{l,m}$	Maximum occupancy of movement (l, m)
$C_{l,m}(t)(\overline{C}_{l,m}(t))$	Saturation flow of movement (l, m) at time t (with a mean of $C_{l,m}(t)$)
$d_{l,m}(t)$	Demand for entry movement $(l, m) \in \mathcal{L}_{\text{enter}}$ at time t
$f_{l,m}$	Average flow for movement (l, m) at time t
$R_{l,m}(t)$	Turning ratio from link l to link m at time t
$\rho^p(t)$	Average density of the busy region at time t
$\rho^i_{l,m}(t)$	Average density of the link cluster inside the protected region associated with movement (l, m). i is an index, called the order of clusters, determining the size of clusters
Ψ	A positive and increasing function reflecting traffic conditions both on local inbound movement and in protected region
Max Pressure control algorithm	
$w_{l,m}(t)$	Weight of movement (l, m) at time t. Superscripts used to differentiate MP algorithms
$p(S^{ij})(t)$	Pressure of phase S^{ij} at time t. Superscripts used to differentiate MP algorithms
$S^*_i(t)$	Signal phase activated at intersection i at time t. Superscripts used to differentiate MP algorithms
Macroscopic Fundamental Diagram	
ρ^p_{cr}	Average density of the protected region

All time step-based MP algorithms[1] apply the following steps to determine signal timings:

1. Retrieve the value of a pre-selected metric – such as queue length, travel time and travel delay – for each vehicle movement, defined as a pair of adjacent links that allow vehicle transitions between them. In most cases, this measurement occurs at the end of the previous time step and measures conditions either at that moment or experienced during the previous time step.

[1]Based on whether the signals follow a cyclical phase structure, MP algorithms can be classified as time step-based in which signal timing is updated every pre-defined time step – as in (Varaiya, 2013), and cycle-based in which signal timing is updated every cycle – as in (Levin et al., 2020). This paper focuses on the former type.

2. Calculate the *weight* for each movement, defined as the difference between the value of the metric for that movement and the average value over its downstream movements.
3. Compute the *pressure* for each phase, defined as the sum of the weight multiplied by the corresponding saturation flow over all movements served by this phase.
4. Activate the phase with the maximum pressure for the next time step.

The rest of this section first reviews D-MP proposed in (Liu and Gayah, 2022) and then develops N-MP and proves its maximum stability property.

2.1. D-MP

Consider a network consisting of a set of nodes $\mathcal{N}$ and a set of directional links $\mathcal{L}$, which can be divided into:

- entry links $\mathcal{L}_{\text{enter}}$, from where vehicles enter the network
- exit links $\mathcal{L}_{\text{exit}}$, from where vehicles exit the networks
- other internal links $\mathcal{L}_{\text{internal}}$

A movement is defined as a pair of adjacent links (l, m) that allows vehicle transitions from link l to m. Let $\mathcal{M}^i$ denote the set of movements at intersection i, and $\mathcal{S}^i$ denote the set of feasible phases at intersection i. Phase j at intersection i, denoted by $S^{ij} \in \mathcal{S}^i$, is an array with a length equal to $|\mathcal{M}^i|$. Each element, $S^{ij}_{l,m}$, is a binary variable indicating if movement (l, m) is served by S^{ij}.

In the D-MP, vehicles on all links are categorized into two groups: moving vehicles, indicated by the green and blue vehicles in Figure 1, and stopped vehicles, indicated by the numbers in the open-end boxes in Figure 1. For simplicity of modeling, we assume that all moving vehicles are traveling at free flow speed, v_f, and all stopped vehicles are waiting at the stop line (the downstream end of the link). In addition, similar to (Varaiya, 2013), the stopped vehicles are modeled by point queues which do not occupy physical space, so the number of stopped vehicles can rise infinitely if the control strategy is not effective. This treatment is related to the maximum stability property, which will be elaborated in the related proof for the N-MP. Under these assumptions, the delay incurred by a movement in a time step is equal to the number of stopped vehicles multiplied by the step size. In addition, the number of moving vehicles is upper bounded. The proof for both statements can be found in (Liu and Gayah, 2022).

2.1.1. Traffic dynamics

Traffic dynamics for both vehicle groups is modeled using store-and-forward models. The evolution of stopped vehicles of a movement (l, m) can be expressed as

$$x^s_{l,m}(t+1) = x^s_{l,m}(t) + x^{m\to s}_{l,m}(t+1) - x^{s\to \text{dis}}_{l,m}(t+1) \tag{1}$$

where $x^s_{l,m}(t)$ is the number of stopped vehicles using movement (l, m) at time t, $x^{m\to s}_{l,m}(t+1)$ is the number of moving vehicles at time t that will join stopped vehicles at time $t+1$ and $x^{s\to dis}_{l,m}(t+1)$ is the number of stopped vehicles that will leave the movement at time $t+1$. Note we use superscripts to denote the moving status and subscripts to denote the movements. $x^{m\to s}_{l,m}(t+1)$ can be expressed as:

$$x^{m\to s}_{l,m}(t+1) = \max\left(0, x^{m'}_{l,m}(t) - \max(0, C_{l,m}(t)S_{l,m}(t) - x^s_{l,m}(t))\right) \tag{2}$$

where $x^{m'}_{l,m}(t)$ indicates the number of moving vehicles (with free flow speed) that can arrive the stop line within one time step, $C_{l,m}(t)$ denotes the stochastic and upper bounded saturation flow with mean value equal to $\overline{C_{l,m}}(t)$ and $S_{l,m}(t)$ is a binary variable indicating if movement (l, m) is served at time t. Some vehicles in $x^{m'}_{l,m}(t)$ may leave the link without stopping if the signal is green and the number of stopped vehicles is less than the saturation flow. Therefore, we should subtract these vehicles, which is equal to $\max(0, C_{l,m}(t)S_{l,m}(t) - x^s_{l,m}(t))$, from $x^{m'}_{l,m}(t)$ to obtain the number of moving vehicles that could join the

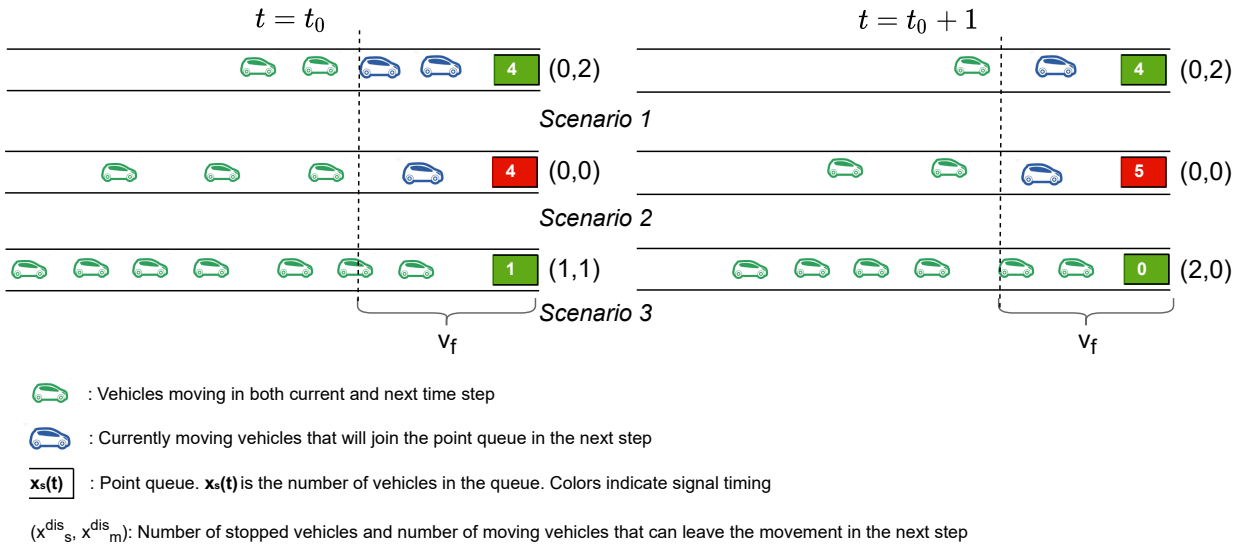

Figure 1: Evolution of traffic for both vehicle groups.

stopped vehicles. Therefore, $x^{m'}_{l,m}(t) - x^{m\to s}_{l,m}(t+1)$ is the number of moving vehicles that will leave the link without stopping, as indicated by the first number inside the parentheses in Figure 1.

This can be explained using Figure 1, which shows the traffic evolution between two consecutive time steps for three scenarios. The color of the open-end boxes indicate the signal timing, and the numbers inside indicate the queue length, i.e., $x^s_{l,m}(t)$. Both green and blue vehicles are moving vehicles, i.e., $x^m_{l,m}(t)$. The moving vehicles within v_f distance from the stop line – i.e., the ones have passed the dashed lines – can arrive the stop line within the current time step; these are included in $x^{m'}_{l,m}(t)$. However, it is possible that only the blue vehicles will join the stopped vehicles in the next step and make up $x^{m\to s}_{l,m}(t+1)$. To see why, assume the saturation flow is 2 veh/step for all three scenarios. For scenarios 1 and 2, since the saturation flow is not high enough to clear the stopped vehicles (scenario 1) or the signal is red (scenario 2), all vehicles within v_f distance from the stop line will join the queue in the next time step, i.e., $x^{m\to s}_{l,m}(t+1) = x^{m'}_{l,m}(t)$. For scenario 3, however, the signal is green and there is only 1 (0) stopped vehicles at $t = t_0$ ($t = t_0 + 1$), so vehicles within v_f distance can leave the link without stopping, i.e, $x^{m\to s}_{l,m}(t+1) = 0 < x^{m'}_{l,m}(t)$. Thus, $x^{s\to dis}_{l,m}(t+1)$ can be expressed as:

$$x^{s\to dis}_{l,m}(t+1) = \min(C_{l,m}(t)S_{l,m}(t), x^s_{l,m}(t)) \tag{3}$$

which is the minimal value between the saturation flow (considering signal timing) in one step and the number of stopped vehicles. This is indicated by the second number inside the parentheses in Figure 1.

The evolution of moving vehicles can be expressed as:

$$x^m_{l,m}(t+1) = x^m_{l,m}(t) - x^{m'}_{l,m}(t) + \sum_{k\in\mathcal{IN}_l} x^{total\to dis}_{k,l}(t+1)R_{l,m}(t+1)\mathbb{1}_{\mathcal{L}_{internal}}(l,m) + d_{l,m}(t+1)\mathbb{1}_{\mathcal{L}_{enter}} \tag{4}$$

where $x^m_{l,m}(t)$ is the number of moving vehicles of movement (l,m) at time t; $\mathcal{IN}_l$ is the set of incoming links of link l; $x^{total\to dis}_{k,l}$ is the total number of vehicles that will leave the movement (k,l), which is equal to the sum of $x^{s\to dis}_{k,l}(t+1)$ and $x^{m\to dis}_{k,l}(t+1)$; $R_{l,m}(t+1)$ is the stochastic turning ratio from link l to link m; and $\mathbb{1}_{(.,.)}(.)$ is the indicator function. The third term is the total inflow from all upstream movements for movement (l,m) if l is an internal link. $d_{l,m}(t+1)$ is the demand of movement (l,m) if l is an entry link. The evolution of total number of vehicles of a movement can be obtained by the sum of (1) and (4):

$$x_{l,m}(t+1) = x_{l,m}(t) - x_{l,m}^{total\to dis}(t+1) + \sum_{k\in\mathcal{IN}_l} x_{k,l}^{total\to dis}(t+1) R_{l,m}(t+1) \mathbb{1}_{\mathcal{L}_{internal}}(l,m) + d_{l,m}(t+1)\mathbb{1}_{\mathcal{L}_{enter}} \tag{5}$$

2.1.2. Signal control algorithm

The D-MP algorithm updates the signal timing for all intersections at a fixed frequency, T, by following the steps introduced at the beginning of this section. First, the delay for all movements incurred in the previous time step is measured. Second, the weight for a movement at each signal update instant can be expressed as:

$$w_{l,m}^D(t) = \sum_{t'=1}^{T} x_{l,m}^s(t-T+t') - \sum_{n\in\mathcal{OUT}_m} \left[\sum_{t'=1}^{T} x_{m,n}^s(t-T+t')\right] R_{m,n}(t) \quad \forall(l,m) \tag{6}$$

where $\mathcal{OUT}_m$ is the set of outgoing links from link m. As mentioned above, the delay incurred by a movement is equivalent to its number of stopped vehicles. Therefore, the first term in Eq. (6) is the delay incurred by movement (l,m) between $t-T+1$ and t. The second term is the average delay over all downstream movements in the same period using turning ratio as the proportions.

Third, the pressure for the jth phase at intersection i, is computed by:

$$p^D(S^{ij})(t) = \sum_{(l,m)\in\mathcal{M}^i} \overline{C_{l,m}}(t) w_{l,m}^D(t) S_{l,m}^{ij}, \quad \forall i,j \tag{7}$$

Fourth, D-MP activates the phase with the maximum pressure at each intersection, i.e.,

$$S_i^{D*}(t) = \arg\max_j p^D(S^{ij})(t), \quad \forall i \tag{8}$$

Eqs. (6)–(8) are repeated every T steps. Next, built upon D-MP, N-MP is proposed in the following section.

2.2. Network MP

The mechanism behind N-MP is to reduce the weight for intersection movements leading into a protected region when it is congested, i.e., when $\rho^p(t) > \rho_{cr}^p$, where $\rho^p(t)$ is the average density of the protected region, and ρ_{cr}^p is the critical average density of the protected region at which the network-level productivity is maximized. As a result, the pressure of phases serving such movements is reduced, which in turn reduces the green time. A general form of the weight of N-MP can be expressed as:

$$w_{l,m}^N(t) = w_{l,m}^D(t) - \Psi(t)\, \mathbb{1}_{(\rho_{cr}^p,+\infty)}(\rho^p(t)) \mathbb{1}_{\mathcal{M}^p}(l,m), \quad \forall(l,m) \tag{9}$$

where $\mathcal{M}^p$ is the set of the inbound movements, and Ψ is a positive function reflecting the current status of both the local intersection and the protected region. In general, the weight reduction should increase with the density in the protected region, $\rho^p(t)$, and it should be higher for the movements with more vehicles waiting to enter the protected region. Both requirements can help mitigate the congestion more efficiently.

Then, the pressure and optimal signal timing from N-MP can be defined as:

$$p^N(S^{ij})(t) = \sum_{(l,m)\in S_{ij}} \overline{C_{l,m}}(t) w_{l,m}^N(t) S_{l,m}^{ij}, \quad \forall i,j \tag{10}$$

$$S_i^{N*}(t) = \arg\max_j p^N(S^{ij})(t), \quad \forall i \tag{11}$$

Note a phase may serve both inbound movements and non-inbound movements, but the weight reduction in Eq. (9) is only implemented for the inbound movements when the protected region is congested, as indicated by the two indicator functions. Next, two forms of the N-MP algorithms are proposed.

2.2.1. Basic N-MP

The weight for the first proposed form of the N-MP algorithm is:

$$w^N_{l,m}(t) = w^D_{l,m}(t) - \Psi\left(\rho^p(t) - \rho^p_{cr},\ x_{l,m}(t)\right) \mathbb{1}_{(\rho^p_{cr},+\infty)}(\rho^p(t)) \mathbb{1}_{\mathcal{M}^p}(l,m), \quad \forall (l,m) \tag{12}$$

For an inbound movement, Ψ is a positive and increasing function of the number of vehicles on the corresponding movement, $x_{l,m}(t)$, and the exceeded density, $\rho^p(t) - \rho^p_{cr}$, in the protected region. The latter factor is identical for all inbound movements. For simplicity, this algorithm is referred to as basic N-MP.

It should be noted that although the basic N-MP requires the average density of the protected region, this value can be easily obtained from the number of vehicles over all intersections in the protected region, which is already available from D-MP. Therefore, the basic N-MP does not require extra data collection. In addition, adding the second term in Eq. (12) does not change the computational complexity and the control architecture. Therefore, N-MP is still a decentralized MP control strategy. Lastly, the second term in Eq. (12) is implemented for inbound movements only if the average density in the protected region exceeds the critical value; otherwise, the weight from D-MP in Eq. (6) is applied.

2.2.2. Clustered N-MP

The term $(\rho^p(t) - \rho^p_{cr})$ in Eq. (12) is identical for all inbound movements, which implies that the same level of restriction resulting from the congestion in the protected region is applied at all inbound movements. This treatment is suitable when the protected region is homogeneously congested. However, when the protected region is relatively large and/or the travel demand is not uniformly distributed over the protected region, such homogeneity cannot be ensured; e.g., see (Daganzo et al., 2011). In addition, since the signal timing of the N-MP is updated at small, regular time steps, (e.g., every 10 s), the area within the protected region that is reasonably influenced by a green inbound movement may be much smaller than the entire region. Under this situation, it is more reasonable to only consider the traffic state in some smaller "clusters" within the protected region as opposed to the entire region. Therefore, the average density of the entire protected region, $\rho^p(t)$ in Eq. (12), can be replaced with the average density of the associated cluster for each perimeter intersection. We refer to this algorithm as the clustered N-MP. This method generates lower (higher) weight reductions for the intersection if the downstream cluster is less (more) congested. Doing so may also help improve congestion homogeneity within the protected region and, thus, may improve overall network efficiency. The weight for the clustered N-MP can be expressed as:

$$w^{CN}_{l,m}(t) = w^D_{l,m}(t) - \Psi\left(\rho^i_{l,m}(t) - \rho^p_{cr},\ x_{l,m}(t)\right) \mathbb{1}_{(\rho^p_{cr},+\infty)}(\rho^p(t)) \mathbb{1}_{\mathcal{M}^p}(l,m), \quad \forall (l,m) \tag{13}$$

where $\rho^i_{l,m}(t)$ is the average density of the cluster associated with movement (l,m), and index i, which is called the order of clusters, determines the size of the clusters. The cluster is defined as a set of links constituting shortest paths to any intersection in the protected region with a length less than i links. Figure 2 shows an example of the cluster for all inbound movements from the target perimeter intersection when $i = 3$. We assume, in general, vehicles travel on shortest travel distance paths, so only the traffic state on such links will be impacted by the corresponding inbound movements at the current step. Consequently, only these links are included in the clusters. Note, if a link is not on the shortest path from the target perimeter intersection to the downstream node of the link, it will not be included in the cluster even if the distance is shorter than i links. For example, all southbound links are not on such shortest paths for the example intersection in Figure 2, and thus, they are not in the cluster.

2.3. Maximum stability property

This section demonstrates that the N-MP algorithms inherit the desirable maximum stability property, if the function Ψ is bounded. We first define other necessary notations for this property and the proof.

Given the demand of entry links $\boldsymbol{d}$ and the turning ratio at all intersections $\boldsymbol{R}$, the average flow $\boldsymbol{f}$ for all movements can be uniquely determined. For simplicity, we omit the expression of $\boldsymbol{f}$ since it does not affect the maximum stability property; however, it can be found in (Liu and Gayah, 2022; Hao et al., 2018).

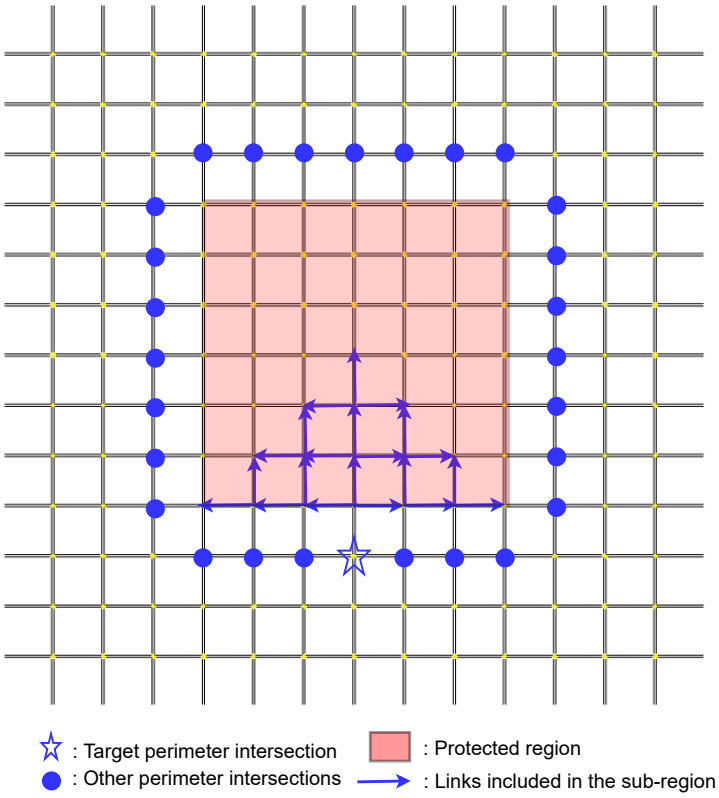

Figure 2: Cluster with an order of 3.

Definition 1. *A feasible signal control sequence* $\{\boldsymbol{S}(t), t = 0, T, 2T, 3T, ...\}$ *can accommodate demand* $\boldsymbol{d}$ *(or equivalently demand* $\boldsymbol{d}$ *is feasible) if*

$$\bar{C}_{l,m}\bar{\Omega}_{l,m} \geq f_{l,m}, \quad \forall(l,m) \tag{14}$$

where $\bar{C}_{l,m}$ *is the mean of the saturation flow of movement* (l,m)*, and* $\bar{\Omega}_{l,m}$ *is the proportion of time that movement* (l,m) *is served under the control sequence, which can be expressed as:*

$$\bar{\Omega}_{l,m} = \liminf_{N\to\infty} \frac{1}{N} \sum_{n=0}^{N} \boldsymbol{S}_{l,m}(nT), \quad \forall(l,m) \tag{15}$$

Definition 1 indicates that a control sequence can accommodate a demand if the average service rate is not lower than the average demand for all movements in the network.

The convex hull of the feasible phases at intersection i can be defined as

$$co(\mathcal{S}^i) = \{\sum_j \lambda_j S^{ij} | \lambda_j \geq 0, \sum_j \lambda_j = 1\} \tag{16}$$

Proposition 1. $\boldsymbol{\Omega} \in co(\mathcal{S})$ *if and only if there exists a feasible control sequence* $\{\boldsymbol{S}(t), t = 0, T, 2T, 3T, ...\}$ *that*

$$\Omega_{l,m} = \lim_{N\to\infty} \frac{1}{N} \sum_{n=0}^{N} \boldsymbol{S}_{l,m}(nT), \quad \forall(l,m) \tag{17}$$

For simplicity, we omit the proof, which can be found in (Varaiya, 2013). By combining Definition 1 and Proposition 1, we can obtain

Proposition 2. *A demand* $\boldsymbol{d}$ *is feasible if there exists a control matrix* $\boldsymbol{\Omega} \in co(\mathcal{S})$ *that*

$$\Omega_{l,m}\bar{C}_{l,m} \geq f_{l,m}, \quad \forall(l,m) \tag{18}$$

Let $\mathcal{D}$ denote the feasible region of demand. For demand on the boundary of $\mathcal{D}$, the Markov chain representing the traffic dynamics can be null recurrent but not positive recurrent. Therefore, we consider the interior of the feasible region, $\mathcal{D}^0$, for which the strict inequality in Eq. (18) holds. Equivalently, when $\boldsymbol{d} \in \mathcal{D}^0$, there exists $\boldsymbol{\Omega} \in co(\mathcal{S})$ and an $\epsilon > 0$ such that

$$\Omega_{l,m}\bar{C}_{l,m} > f_{l,m} + \epsilon, \quad \forall(l,m) \tag{19}$$

Now we define stability mathematically.

Definition 2. *A control policy stabilizes a demand if the average number of vehicles in the network is upper bounded, i.e.,*

$$\exists \nu > 0, \quad \frac{1}{N}\sum_{n=1}^{N}\sum_{l,m} E\{x_{l,m}(nT)\} \leq \nu, \quad \forall N \in Z^+ \tag{20}$$

Note that since the number of vehicles of a movement is modeled by point queue models in (Varaiya, 2013), the queue length of a movement defined in (Varaiya, 2013) is the same as the number of vehicles of that movement. Therefore, Definition 2 is identical with the corresponding definition in (Varaiya, 2013).

Proposition 3. *A control strategy stabilizes a demand if there exist* $k < \infty$ *and* $\tau > 0$ *such that the Lyapunov function* $|\boldsymbol{X}(t)|^2$ *satisfies the following inequality,*

$$E\left[|\boldsymbol{X}(t+T)|^2 - |\boldsymbol{X}(t)|^2 | \boldsymbol{X}(t)\right] \leq k - \tau|\boldsymbol{X}(t)|, \ t = 0, T, 2T, ... \tag{21}$$

where $|\boldsymbol{X}(t)| \equiv \sum_{l,m} x_{l,m}(t)$ *and* $|\boldsymbol{X}(t)|^2 \equiv \sum_{l,m} x_{l,m}^2(t)$.

Proof. The proof is similar to previous studies; e.g., see Varaiya (2013). It is repeated here to make the proof easier to follow.

Taking expectation for both sides of Eq. (21) obtains

$$E[|\boldsymbol{X}(t+T)|^2] - E[|\boldsymbol{X}(t)|^2] \leq k - \tau E[|\boldsymbol{X}(t)|], \ t = 0, T, 2T, ... \tag{22}$$

Then, for any $N \in Z^+$,

$$\sum_{n=0}^{N} E[|\boldsymbol{X}(t+T)|^2] - \sum_{n=0}^{N} E[|\boldsymbol{X}(t)|^2] = E[|\boldsymbol{X}(NT)|^2] - E[|\boldsymbol{X}(0)|^2] \leq Nk - \tau\sum_{n=0}^{N} E[|\boldsymbol{X}(nT)|] \tag{23}$$

Therefore,

$$\frac{1}{N}\sum_{n=0}^{N} E[|\boldsymbol{X}(nT)|] \leq \frac{k}{\tau} + \frac{1}{\tau N}\left[E[|\boldsymbol{X}(0)|^2] - E[|\boldsymbol{X}(NT)|^2]\right] \leq \frac{k}{\tau} + \frac{1}{\tau N}E[|\boldsymbol{X}(0)|^2], \ \forall N \in Z^+ \tag{24}$$

The right-hand side is a positive constant, so Eq. (20) is established. Consequently, Proposition 3 is proved. □

Theorem 1 defines the maximum stability for N-MP.

Theorem 1. *If Ψ is bounded, N-MP stabilizes a demand, $\boldsymbol{d}$, whenever the average demand $\bar{\boldsymbol{d}} \in \mathcal{D}^0$.*

Proof. Proposition 3 shows that a control strategy stabilizes a demand if Eq. (21) is established. Therefore, we focus on the proof of Eq. (21) under the control of N-MP. Without loss of generality, assume T is the free flow travel time on a link. Longer links can be divided into shorter segments; see (Varaiya, 2013; Levin et al., 2020). Eq. (5) becomes

$$\begin{aligned} x_{l,m}(t+T) =& x_{l,m}(t) - \min\left(C_{l,m}(t)S_{l,m}(t), x_{l,m}(t)\right) \\ &+ \sum_{k\in\mathcal{IN}_l} \min\left(C_{k,l}(t)S_{k,l}(t), x_{k,l}(t)\right) R_{l,m}(t+1)\mathbb{1}_{\mathcal{L}_{internal}}(l,m) + d_{l,m}(t+1)\mathbb{1}_{\mathcal{L}_{enter}} \end{aligned} \tag{25}$$

Let $\boldsymbol{\delta}(t+T)$ denote the array of the difference of the number of vehicles between two consecutive steps. Then,

$$\begin{aligned} \delta_{l,m}(t+T) =& x_{l,m}(t+T) - x_{l,m}(t) \\ =& -\min\left(C_{l,m}(t)S_{l,m}(t), x_{l,m}(t)\right) \\ &+ \sum_{k\in\mathcal{IN}_l} \min\left(C_{k,l}(t)S_{k,l}(t), x_{k,l}(t)\right) R_{l,m}(t+1)\mathbb{1}_{\mathcal{L}_{internal}}(l,m) + d_{l,m}(t+1)\mathbb{1}_{\mathcal{L}_{enter}} \end{aligned} \tag{26}$$

Then,

$$E\{|\boldsymbol{X}(t+T)|^2 - |\boldsymbol{X}(t)|^2|\boldsymbol{X}(t)\} = 2E\{\boldsymbol{X}(t)^T\boldsymbol{\delta}(t+T)|\boldsymbol{X}(t)\} + E\{|\boldsymbol{\delta}(t+T)|^2|\boldsymbol{X}(t)\} = 2\alpha + \beta \tag{27}$$

where

$$\begin{aligned} \alpha =& -E\left\{\sum_{l,m} x_{l,m}(t)\min\left(C_{l,m}(t)S_{l,m}(t), x_{l,m}(t)\right)|\boldsymbol{X}(t)\right\} \\ &+ E\left\{\sum_{l,m} x_{l,m}(t)\left(\sum_{k\in\mathcal{IN}_l}\min\left(C_{l,m}(t)S_{l,m}(t), x_{l,m}(t)\right)R_{l,m}(t+1)\mathbb{1}_{\mathcal{L}_{internal}}(l,m) + d_{l,m}(t+1)\mathbb{1}_{\mathcal{L}_{enter}}\right)|\boldsymbol{X}(t)\right\} \\ =& \sum_{l,m}\left[f_{l,m} - E\left[\min\left(C_{l,m}(t)S_{l,m}(t), x_{l,m}(t)\right)|\boldsymbol{X}(t)\right]\right]w^Q_{l,m}(t) \end{aligned} \tag{28}$$

where $w^Q_{l,m}$ is the weight defined in (Varaiya, 2013), which can expressed as

$$w^Q_{l,m}(t) = x_{l,m}(t) - \sum_{n\in\mathcal{OUT}_m} x_{m,n}(t)R_{m,n}(t) \quad \forall(l,m) \tag{29}$$

and

$$\begin{aligned} \beta =& \sum_{l,m} E\Big\{\Big[-\min\left(C_{l,m}(t)S_{l,m}(t), x_{l,m}(t)\right) \\ &+ \sum_{k\in\mathcal{IN}_l}\min\left(C_{k,l}(t)S_{k,l}(t), x_{k,l}(t)\right)R_{l,m}(t+1)\mathbb{1}_{\mathcal{L}_{internal}}(l,m) + d_{l,m}(t+1)\mathbb{1}_{\mathcal{L}_{enter}}\Big]^2|\boldsymbol{X}(t)\Big\} \end{aligned} \tag{30}$$

The derivation of the second equality of Eq. (28) can be found in (Varaiya, 2013), which is omitted from this paper for simplicity.

Lemma 1. *β is upper bounded by a constant regardless of the control policy.*

Proof. Since the saturation flow $C_{l,m}(t)$ and average demand at the entry links $d_{l,m}(t+1)$ are both upper bounded, and $S_{l,m}(t)$ is a 0-1 function, all three terms inside the expectation of Eq. (30) are upper bounded by a constant. Therefore, β is upper bounded by a constant regardless of the control policy. □

Lemma 2. *If Ψ is bounded, there exist $\tau > 0$ and $\kappa < \infty$ such that α is upper bounded by $-\tau|\boldsymbol{X}(t)| + \kappa$ under N-MP.*

Proof. From Eq. (28), we obtain

$$\begin{aligned}\alpha =& \sum_{l,m} \left[f_{l,m} - \bar{C}_{k,l}(t) S^{N*}_{l,m}(t)\right] w^{Q}_{l,m}(t) + \sum_{l,m} \left[\bar{C}_{k,l}(t) S^{N*}_{l,m}(t) - E\left[\min\left(C_{l,m}(t) S^{N*}_{l,m}(t), x_{l,m}(t)\right)|\boldsymbol{X}(t)\right]\right] w^{Q}_{l,m}(t) \\ =& \alpha_1 + \alpha_2\end{aligned} \tag{31}$$

Using the conditions that $S^{N*}_{l,m}(t)$ is a 0-1 function, and $w^{Q}_{l,m}(t) \leq x_{l,m}(t)$, it is easy to prove that

$$\alpha_2 \leq \bar{\boldsymbol{C}}^T \boldsymbol{C^u} = \kappa_1 \tag{32}$$

where $\boldsymbol{C^u}$ is the array of the upper bounds of saturation flow of all movements. The proof can be found in (Liu and Gayah, 2022), which is omitted from this paper for simplicity. Note that Lemma 1 and Eq. (32) are only dependent on the store-and-forward model Eq. (5) regardless of the control policy. Therefore, all MP algorithms using the same traffic dynamics model have the similar proofs for both α_2 and β. The control policy only impacts the proof for α_1.

Eq. (1) leads to

$$x^{s}_{l,m}(t-1) = x^{s}_{l,m}(t) - x^{m\to s}_{l,m}(t) + x^{s\to dis}_{l,m}(t) = x^{s}_{l,m}(t) + z^{s}_{l,m}(t-1,t) \tag{33}$$

As mentioned in Section 2.1, $x^{m\to s}_{l,m}(t)$ and $x^{s\to dis}_{l,m}(t)$ are upper bounded, so $z^{s}_{l,m}(t-1,t)$, which indicates the change in the number of stopped vehicles from time $t-1$ to t, is upper bounded. Using the same manner, we can obtain

$$x^{s}_{l,m}(t-I) = x^{s}_{l,m}(t) + \sum_{i=1}^{I} z^{s}_{l,m}(t-i, t-i+1) = x^{s}_{l,m}(t) + Z^{s}_{l,m}(t-I,t), \forall I \in Z^{+} \tag{34}$$

Let $Z^{s}_{l,m}(t,t) = 0,\ \forall t$, we have

$$x^{s}_{l,m}(t-I) = x^{s}_{l,m}(t) + Z^{s}_{l,m}(t-I,t), \forall I \in Z^{*} \tag{35}$$

where Z^{*} is the set of non-negative integers.

Substituting Eq. (35) into (6) gives

$$
\begin{aligned}
w^D_{l,m}(t) =& \sum_{t'=1}^{T} x^s_{l,m}(t-T+t') - \sum_{n\in\mathcal{OUT}_m}\left[\sum_{t'=1}^{T} x^s_{m,n}(t-T+t')\right] R_{m,n}(t)\\
=& \sum_{t'=1}^{T}\left[x^s_{l,m}(t) + Z^s_{l,m}(t-T+t',t)\right] - \sum_{n\in\mathcal{OUT}_m}\left[\sum_{t'=1}^{T} x^s_{m,n}(t) + Z^s_{m,n}(t-T+t',t)\right] R_{m,n}(t)\\
=& \sum_{t'=1}^{T}\left[x^s_{l,m}(t) + x^m_{l,m}(t)\right] - \sum_{n\in\mathcal{OUT}_m}\left[\sum_{t'=1}^{T}(x^s_{m,n}(t) + x^m_{m,n}(t))\right] R_{m,n}(t)\\
&+ \sum_{t'=1}^{T}\left[Z^s_{l,m}(t-T+t',t) - x^m_{l,m}(t)\right] - \sum_{n\in\mathcal{OUT}_m}\left[\sum_{t'=1}^{T} Z^s_{m,n}(t-T+t',t) - x^m_{m,n}(t)\right] R_{m,n}(t)\\
=& \sum_{t'=1}^{T} x_{l,m}(t) - \sum_{n\in\mathcal{OUT}_m}\sum_{t'=1}^{T} x_{m,n}(t) R_{m,n}(t) + \Phi_{l,m}(t)\\
=& T w^Q_{l,m}(t) + \Phi_{l,m}(t)
\end{aligned}
\tag{36}
$$

where

$$
\Phi_{l,m}(t) = \sum_{t'=1}^{T}\left[Z^s_{l,m}(t-T+t',t) - x^m_{l,m}(t)\right] - \sum_{n\in\mathcal{OUT}_m}\left[\sum_{t'=1}^{T} Z^s_{m,n}(t-T+t',t) - x^m_{m,n}(t)\right] R_{m,n}(t) \tag{37}
$$

Since $Z^s_{l,m}$ and $x^m_{l,m}$ are upper bounded by constants, Φ is upper bounded by a constant. Following Eq. (36) and Eq. (12), α_1 in Eq. (31) can be expressed as:

$$
\begin{aligned}
\alpha_1 =& \sum_{l,m}\left[f_{l,m} - \bar{C}_{k,l}(t) S^{N*}_{l,m}(t)\right] w^Q_{l,m}(t)\\
=& \frac{1}{T}\sum_{l,m}\left[f_{l,m} - \bar{C}_{k,l}(t) S^{N*}_{l,m}(t)\right]\left(w^D_{l,m}(t) - \Phi_{l,m}(t)\right)\\
=& \frac{1}{T}\sum_{l,m}\left[f_{l,m} - \bar{C}_{k,l}(t) S^{N*}_{l,m}(t)\right]\left(w^N_{l,m}(t) + \Psi_{l,m}(t)\mathbb{1}_{(\rho^p_{cr},+\infty)}(\rho^p(t))\mathbb{1}_{\mathcal{M}^p}(l,m) - \Phi_{l,m}(t)\right)
\end{aligned}
\tag{38}
$$

Since the demand is in the interior of the stable region, i.e., $\bar{\boldsymbol{d}} \in \mathcal{D}^0$, Proposition 2 indicates that there exists a control matrix $\boldsymbol{\Omega} \in co(\mathcal{S})$ and an $\epsilon > 0$ such that

$$
\bar{C}_{k,l}(t)\Omega_{l,m}(t) \geq \begin{cases} f_{l,m} + \epsilon, & \text{if } w^N_{l,m}(t) > 0 \quad (39a)\\ 0 & \text{otherwise} \quad (39b)\end{cases}
$$

In addition, according to Eq. (11), $\boldsymbol{S^{N*}}$ maximizes $\sum_{l,m}\bar{C}_{k,l}(t)S_{l,m}(t)w^N_{l,m}(t)$ over all feasible control matrices, i.e., $\forall \boldsymbol{S}(t) \in \mathcal{S}$. Since any feasible control matrix is a corner point or on the boundary of the convex hull, and $\sum_{l,m}\bar{C}_{k,l}(t)S_{l,m}(t)w^N_{l,m}(t)$ is a linear function of $S_{l,m}(t)$, according to the fundamental theorem of linear programming, $\boldsymbol{S^{N*}}$ also maximizes this function over all control matrices in the convex hull, i.e., $\forall \boldsymbol{\Omega} \in co(\mathcal{S})$. Therefore,

$$
\begin{aligned}
\alpha_1 =& \frac{1}{T}\sum_{l,m}\left[f_{l,m}-\bar{C}_{k,l}(t)S^{N*}_{l,m}(t)\right]\left(w^N_{l,m}(t)+\Psi_{l,m}(t)\mathbb{1}_{(\rho^p_{cr},+\infty)}(\rho^p(t))\mathbb{1}_{\mathcal{M}^p}(l,m)-\Phi_{l,m}(t)\right)\\
\leq& \frac{1}{T}\sum_{l,m}\left[f_{l,m}-\bar{C}_{k,l}(t)\Omega_{l,m}(t)\right]\left(w^N_{l,m}(t)+\Psi_{l,m}(t)\mathbb{1}_{(\rho^p_{cr},+\infty)}(\rho^p(t))\mathbb{1}_{\mathcal{M}^p}(l,m)-\Phi_{l,m}(t)\right)\\
\leq& \frac{1}{T}\sum_{\{(l,m):w^N_{l,m}(t)>0\}} -\epsilon\left(w^N_{l,m}(t)+\Psi_{l,m}(t)\mathbb{1}_{(\rho^p_{cr},+\infty)}(\rho^p(t))\mathbb{1}_{\mathcal{M}^p}(l,m)-\Phi_{l,m}(t)\right)\\
&+\frac{1}{T}\sum_{\{(l,m):w^N_{l,m}(t)\leq 0\}} f_{l,m}\left(w^N_{l,m}(t)+\Psi_{l,m}(t)\mathbb{1}_{(\rho^p_{cr},+\infty)}(\rho^p(t))\mathbb{1}_{\mathcal{M}^p}(l,m)-\Phi_{l,m}(t)\right)\\
\leq& -\frac{\epsilon}{T}|\boldsymbol{w}^N(t)|+\frac{1}{T}\sum_{l,m}\left(\Psi_{l,m}(t)\mathbb{1}_{(\rho^p_{cr},+\infty)}(\rho^p(t))\mathbb{1}_{\mathcal{M}^p}(l,m)-\Phi_{l,m}(t)\right)
\end{aligned}
\tag{40}
$$

It has been shown (Varaiya, 2013; Liu and Gayah, 2022) that there exists $\eta > 0$ such that, $|\boldsymbol{w}^Q(t)| \geq \eta|\boldsymbol{X}(t)|$. Since $w^N_{l,m}(t) = w^Q_{l,m}(t) - \Psi_{l,m}(t) + \Phi_{l,m}(t)$, and $\Psi_{l,m}(t)$ and $\Phi_{l,m}(t)$ are upper bounded by a constant, there exists $\gamma < \infty$ such that

$$
|\boldsymbol{w}^N(t)| \geq |\boldsymbol{w}^Q(t)| + \gamma \geq \eta|\boldsymbol{X}(t)| + \gamma \tag{41}
$$

Therefore,

$$
\begin{aligned}
\alpha_1 \leq& -\frac{\epsilon}{T}|\boldsymbol{w}^N(t)|+\frac{1}{T}\sum_{l,m}\left(\Psi_{l,m}(t)\mathbb{1}_{(\rho^p_{cr},+\infty)}(\rho^p(t))\mathbb{1}_{\mathcal{M}^p}(l,m)-\Phi_{l,m}(t)\right)\\
\leq& -\frac{\epsilon}{T}(\eta|\boldsymbol{X}(t)|+\gamma)+\frac{1}{T}\sum_{l,m}\left(\Psi_{l,m}(t)\mathbb{1}_{(\rho^p_{cr},+\infty)}(\rho^p(t))\mathbb{1}_{\mathcal{M}^p}(l,m)-\Phi_{l,m}(t)\right)\\
=& -\tau|\boldsymbol{X}(t)|+\kappa_2
\end{aligned}
\tag{42}
$$

Let $\kappa = \kappa_1 + \kappa_2$, combining Eqs. (32) and (42) proves Lemma 2. □

Following Lemma 1 and Lemma 2, the inequality Eq. (21) is established. Consequently, according to Proposition 3, Theorem 1 is proved. □

Note the maximum stability property holds for both basic N-MP and clustered N-MP as long as function Ψ is bounded.

2.4. Implementation of N-MP

The previous section proves that if Ψ in Eqs. (12) and (13) is an upper bounded function and the demand is in the stable region, basic N-MP and clustered N-MP can stabilize the network. To be an effective PC algorithm, this function should also impose higher restriction on the inflows when the protected region is more congested, which implies it should be increasing with ρ^p and $x_{l,m}$ for all inbound movements. Taking this requirement into consideration, the form shown in Eq. (43) is employed for basic N-MP in the rest of this paper

$$
\Psi\left(\rho^p(t)-\rho^p_{cr},\ x_{l,m}(t)\right) = \xi(\rho^p(t)-\rho^p_{cr})^2\left(\frac{1}{1+\exp\left(\frac{-x_{l,m}(t)}{\chi}\right)}-\frac{1}{2}\right)\times 10^3, \quad \forall(l,m) \tag{43}
$$

where ξ and χ are two parameters to adjust the shape of the function. Replace $\rho^p(t)$ with $\rho^i_{l,m}(t)$ for the clustered N-MP. The term in the second parenthesis is a transformation of a sigmoid function, which

is increasing in $x_{l,m}(t)$ and upper bounded by $\frac{1}{2}$. In addition, since this function is activated only if $\rho^p(t) > \rho^p_{cr}$, it is increasing in $\rho^p(t)$ as well. To maintain the maximum stability property, we need the $\rho^p(t)$ to be bounded.

Proposition 4. *For any demand satisfying $\bar{\boldsymbol{d}} \in \mathcal{D}^0$, $\rho^p(t)$ is upper bounded under the control of N-MP.*

Proof. Consider the protected region as a separate network, and the external demand for this network, $\boldsymbol{d}^p$, is equal to the entry flows from all perimeter intersections. Note $\boldsymbol{d}^p$ is uniquely determined by the demand $\boldsymbol{d}$ and the turning ratio matrix $\boldsymbol{R}$ from the whole network.

Let $\boldsymbol{d}^p_D = f(\boldsymbol{d})$ be the demand array for the protected region under the control of D-MP. Since $\bar{\boldsymbol{d}} \in \mathcal{D}^0$, D-MP can stabilize the network. Consequently, D-MP can stabilize the protected region under the demand $\boldsymbol{d}^p_D$.

After implementing N-MP, the perimeter intersections restrict inflows into the protected region. Assuming the turning ratio is not impacted by the control policy, the corresponding demand under the control of N-MP satisfies $\boldsymbol{d}^p_N \leq \boldsymbol{d}^p_D$. Note the intersections inside the protected are still controlled by D-MP. Since D-MP can accommodate $\boldsymbol{d}^p_D$, it can also stabilize the network under the demand of $\boldsymbol{d}^p_N$. Equivalently, according to Definition 2, the average density in the protected region is upper bounded for all steps. □

We can use the same manner to prove that $\rho^i_{l,m}(t)$ is upper bounded under the control of clustered N-MP.

In addition to the boundedness of Ψ to ensure the maximum stability, a modification is made to avoid an unfavorable solution that may arise from the MP algorithms: a phase with all empty upstream movements or all jammed downstream links can have the maximum pressure and, thus, can be selected even though no vehicle can move under this situation. In other words, MP algorithms are not work-conservative (Gregoire et al., 2014; Mercader et al., 2020; Liu and Gayah, 2023). To ensure the work conservation, we add another term shown in Eq. (44) to the pressure calculation,

$$\Upsilon(S^{ij})(t) = -\frac{1}{M\sum_{(l,m)\in S^{ij}}\left(x_{l,m}(t)\sum_{n\in\mathcal{OUT}_m}\left(Q_{m,n} - x_{m,n}(t)\right)\right) + o} \tag{44}$$

where $Q_{m,n}$ is the maximum occupancy of movement (m,n), M is a big positive number and o is a small positive number. The denominator is always positive. If all movements served by phase S^{ij} are empty or have fully occupied downstream links, the term $M\sum_{(l,m)\in S^{ij}}\left(x_{l,m}(t)\sum_{n\in\mathcal{OUT}_m}\left(Q_{m,n} - x_{m,n}(t)\right)\right)$ is equal to 0, and $\Upsilon(S^{ij})(t)$ is a big (in terms of the absolute value) negative number, which ensures this phase will not be selected by the algorithm. On the other hand, if at least one vehicle can be served by this phase, the denominator becomes a big positive number, so the modified pressure is nearly the same as the original pressure. Adding the small number o ensures the boundedness of $\Upsilon(S^{ij})(t)$, so the maximum stability property still holds. The proof is similar to the proof of Theorem 1, so it is omitted for concision.

3. Numerical Experiments

This section demonstrates the performance of the proposed basic N-MP and clustered N-MP via microscopic traffic simulation using the AIMSUN software. Three travel demand patterns are tested. Two perimeter control approaches, which are the bang-bang control (Daganzo, 2007) and the PI feedback control (Keyvan-Ekbatani et al., 2012), are employed as the baseline models. In addition, the effectiveness of both the proposed algorithms and the bang-bang control in a partially connected environment is also studied.

3.1. Network setup

A 13×13 uniform square grid network of two-way streets is used in the simulation, as shown in Figure 3. The length for all links is 200 m. All links have three dedicated lanes, one for each of the left-turn, through and right-turn movement. The saturation flow for each lane was set at 1800 vehicles per hour. The protected region is considered as the 7×7 region at the center of the large network. Correspondingly, the blue dots are the perimeter intersections.

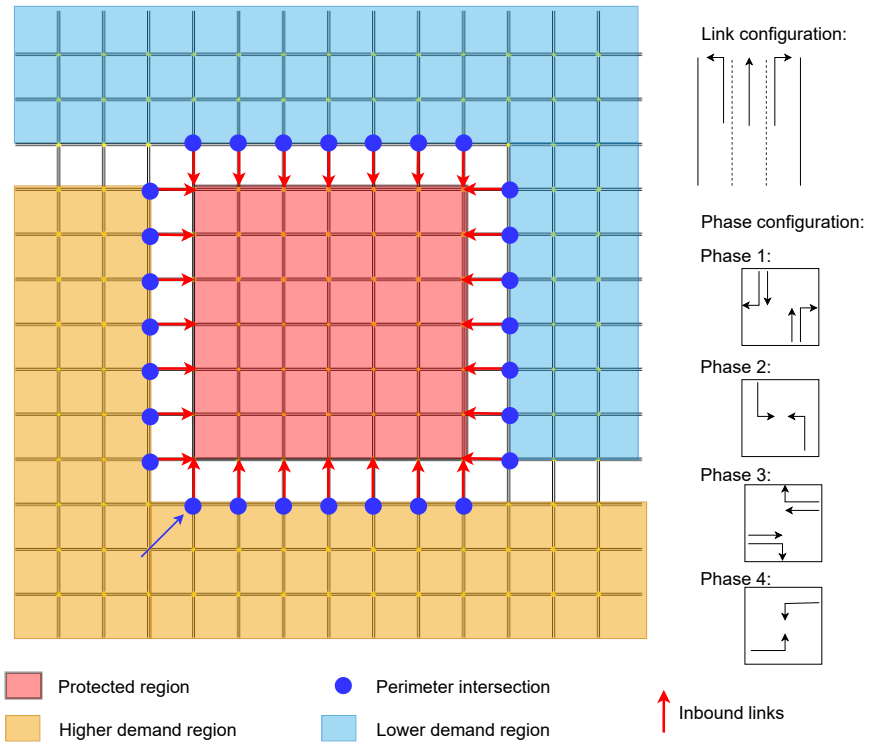

Figure 3: Network setup.

The set for feasible phases shown in Figure 3 are identical for all intersections. The signal update frequency is set to 10 s at all intersections. The yellow time and all-red time are set to 3 s and 1 s, respectively. For each perimeter intersection, there are three inbound movements that are served by distinct phases. For example, the three movements for the intersection marked by the arrow in Figure 3 are indicated by red dashed arrows in Figure 4.

The simulation time is 5 hours, and vehicle positions are updated at regular 1-second intervals. The stochastic c-logit route choice model was used in AIMSUN to emulate user-equilibrium routing conditions in which vehicles make routing decisions to minimize their own personal travel times.

Each intersection serves as a centroid to generate or attract trips. Origins are uniformly distributed over the entire network, while the destinations are uniformly distributed over the protected region. This pattern is used to emulate a mono-centric city during peak hours, which is similar to the pattern used in (Ni and Cassidy, 2019). Three demand scenarios are tested: one uniform demand scenario and two non-uniform demand scenarios with different levels of imbalance. For each case, all destination nodes are equally likely for each trip. However, the scenarios differ based on where the trips are generated. For the first scenario, all origins generate trips at the same average rate, and the specific trip generation pattern over time is shown in Figure 5a. To observe the MFD in the congestion formation and dissipation process, we gradually increase the demand from a very low level to a high level and then gradually decrease it back to the low level. The last 80 minutes with zero demand are used as a cool down period. Note this cool down period is not necessarily long enough to serve all generated vehicles if the signal control strategy is not effective. In the non-uniform demand scenarios, nodes in the orange area of Figure 3 generate trips at a higher rate than those in the blue area. The demand generating ratio between the orange area, red area and blue area is 1.1:1:0.9 (low imbalance), and 1.2:1:0.8 (high imbalance), respectively; see Figs 5b and 5c. Under all three demand patterns, there are an average of 113,190 vehicles generated in one simulation run. To consider the influence of randomness, we run 5 replications with different random starting seeds for each scenario.

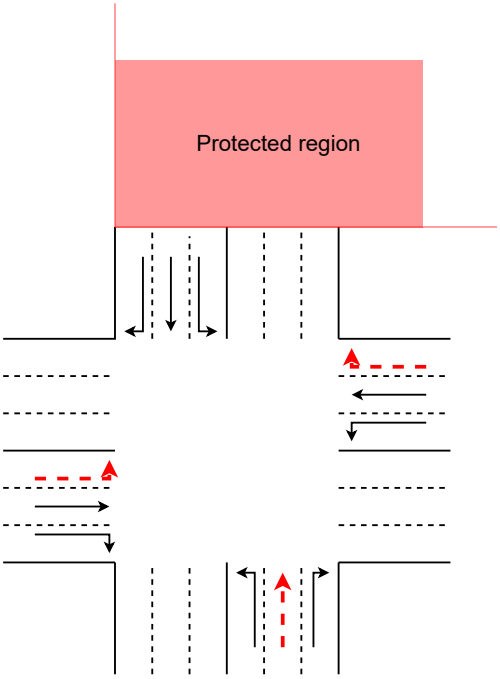

Figure 4: Restricted movements at perimeter intersection.

3.2. Baseline models

We select two popular PC algorithms as the baseline models.

3.2.1. Bang-bang control

The first baseline model is the bang-bang control proposed in (Daganzo, 2007), which has been theoretically demonstrated to maximize the network exit rate if the influence of boundary queues is ignored. To implement this strategy at the perimeter intersections, green-time meters are installed at the downstream end of all inbound lanes of the protected region; e.g., the three lanes marked in Figure 4. When $\rho^p(t) > \rho^p_{cr}$, the meters are set to be red for the next time step; and the perimeter intersections are controlled by D-MP without considering these inbound movements. When $\rho_{in}(t) \leq \rho_c$, the meters turn green, and all perimeter intersections are controlled by regular D-MP. Under this framework, the bang-bang control also maintains the MP control architecture, and the corresponding weight is:

$$w^B_{l,m}(t) = w^D_{l,m}(t)\left(1 - \mathbb{1}_{(\rho^p_{cr},+\infty)}(\rho^p(t))\mathbb{1}_{\mathcal{M}^p}(l,m)\right), \quad \forall (l,m) \tag{45}$$

The term in the parenthesis forces the weights for only the inbound movements to be 0 if $\rho^p(t) > \rho^p_{cr}$; when $\rho^p(t) \leq \rho^p_{cr}$, the weights for all movements are computed from D-MP.

3.2.2. Feedback control

The second baseline model is a feedback control (FC) strategy inspired by the PI feedback control model proposed in (Keyvan-Ekbatani et al., 2012). Unlike the bang-bang control, the PI feedback regulates the inflows for each signal cycle by considering the inflows in the previous cycle, total time spent in two consecutive cycles and the critical total time spent in the protected region. Specifically, the inflows for a cycle can be expressed as:

$$q_{in}(k) = q_{in}(k-1) - K_p[TTS(k) - TTS(k-1)] + K_I[\widehat{TTS} - TTS(k)] \tag{46}$$

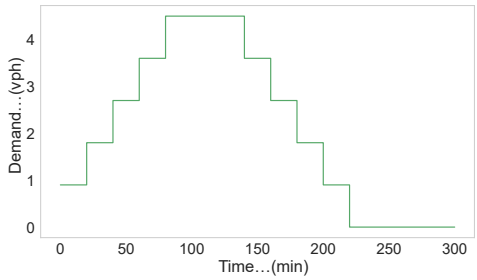

(a) Uniform demand

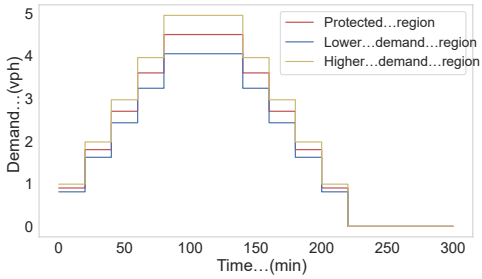

(b) Non-uniform demand with low imbalance

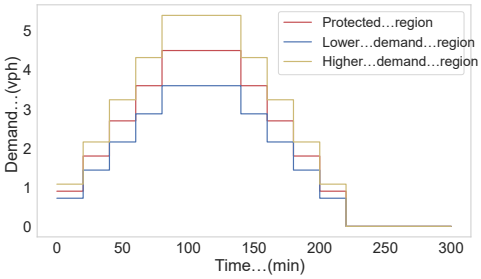

(c) Non-uniform demand with high imbalance

Figure 5: Three demand scenarios.

where K_P and K_I are two non-negative parameters, which are called proportional and integral gains, respectively. $TTS(k)$ is the total time spent in the protected region in cycle k and $\widehat{TTS}$ is the total time spent associated with the critical density in MFD. The controlled inflows need to be split over all perimeter intersections using other algorithms, but the split does not impact the performance significantly as long as the total inflow is roughly followed. In addition, the authors claimed that if the perimeter is applied at the periphery of the protected region, the P gain can be dropped, and an I-type regulator would perform reasonably well.

PI feedback control is based on signal cycles, so it cannot be readily implemented in the simulation as the signal control in the simulation is based on time steps. Therefore, a modified FC algorithm using the similar control logic is proposed. In addition to the signal update frequency of 10 s, we also employ another longer time step (equal to 100 s in this study) to update FC inflows. This longer time step is referred to as time horizon to be distinguished from the signal update frequency. At the beginning of each horizon, the FC algorithm determines the number of 10-s time steps within this horizon that all inbound movements need to be blocked as follows:

$$t_b(k) = t_b(k-1) + K_I(\rho^p(k) - \rho^p_{cr}) \tag{47}$$

where $t_b(k)$ is the number of blocked time steps in horizon k, K_I is the integral gain and $\rho^p(k)$ is the average density of the protected region at the beginning of horizon k, which is correlated to $TTS(k)$. Therefore, Eq. (47) mimics the PI feedback gating under the time step-based framework. The P gain is dropped since the perimeter intersections are at the periphery of the protected region.

3.3. Calibration of MFD and critical density

The critical density of the protected region, ρ^p_{cr}, serves as a critical input for both the proposed algorithm and the baseline models, so we first obtain this parameter from MFDs under the D-MP strategy. The MFD is represented by the relationship between the trip completion rate in the protected region (veh/h) (equivalent to the trip completion rate of the whole network since all destinations are in the protected region) and its

average density (veh/lane-km). The number of vehicles in the network and the number of completed trips are retrieved every second. Then, the density is computed as the number of vehicles divided by the network length, and the network exit rate is computed as the number of completed trips scaled up to an hourly rate. Both the density and trip completion rate are averaged every 100 seconds.

The results of MFD under the three demand scenarios are shown in Figure 6. The general pattern of the three MFDs are similar; however, the variation of the trip completion rate increases with the level of imbalance.

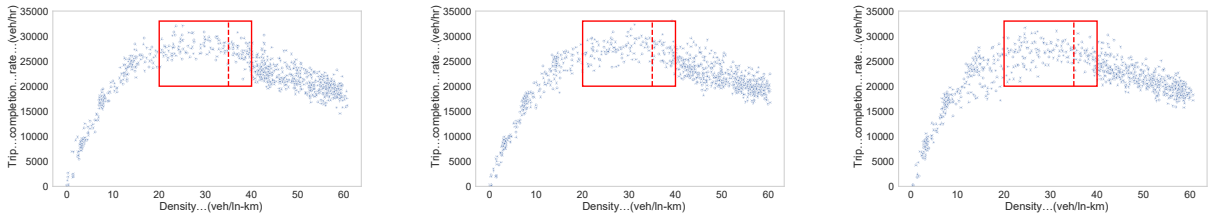

(a) Uniform demand (b) Low imbalance (c) High imbalance

Figure 6: MFD under D-MP.

Figure 6 shows that the trip completion rate reaches its maximum when the average density falls between 20 veh/ln-km and 40 veh/ln-km for all demand scenarios; this range is shown by the red boxes in Figure 6. Next, we identify a value from this range that maximizes the control efficiency of the perimeter control algorithms as ρ_{cr}^{p}. To ensure a fair comparison, only bang-bang control is used for this process, and the following values (veh/ln-km) are tested: 20, 25, 30, 35, 40. The results are shown in Figure 7. The horizontal line $y = 0$ is used as a baseline to indicate the performance of D-MP. The vertical axis is the increase in the cumulative number of vehicles resulting from the bang-bang control compared to D-MP. It clearly shows that bang-bang control can enhance the network efficiency considerably for all demand scenarios. Figure 7 also unveils the inability of current MP algorithms to accommodate congestion in a busy region with heavy external traffic demand. For all three demand scenarios, the vehicle exit rate increases when ρ_{cr}^{p} increases from 20 to 35 and decreases when ρ_{cr}^{p} increases from 35 to 40. When ρ_{cr}^{p} is too small, e.g., 20 veh/ln-km, the bang-bang control starts blocking inflows too early before the network reaches the critical state, which decreases the exit rate for a period after the bang-bang is activated. On the other side, a too large value cannot keep the density below a desired value. Figure 7 shows that $\rho_{cr}^{p} = 30$ and $\rho_{cr}^{p} = 35$ generate similar control performance. We select $\rho_{cr}^{p} = 35$, indicated by the dashed lines in Figure 6, as the critical density for all algorithms in the following.

3.4. Results with full knowledge of traffic states

This section compares the control performance of the basic N-MP, clustered N-MP, bang-bang and FC strategies for the three demand scenarios assuming full and accurate information about the traffic state of the network is available.

First, the two parameters in Eq. (43) are manually tuned. Given the link length of 200 m and the jam density of around 200 veh/lane-km, $x_{l,m}(k)$ is in the range between 0 and 40. χ determines the shape of the modified sigmoid function in this range. After testing different magnitudes, a relatively large number, 400, is selected to make this term roughly linear with respected to $x_{l,m}(k)$ in this range, as shown in Figure 8.

In addition, ten integers from 1 to 10 are tested for ξ in Eq. (43). Figure 9 shows the corresponding results from the basic N-MP. For the purpose of visualization, only five values are shown in each figure. The left column shows the improvement from the basic N-MPs compared to D-MP are similar for all tested values, which implies the basic N-MP is relatively stable under the change of ξ with the tested range. Note when $\xi = 0$, the basic N-MP is identical to the D-MP. To have a better comparison between the tested values, the right column shows the results using the ξ value that generates the worst performance as the baseline. Although the difference in the exit vehicles between different values of ξ is relatively small compared to actual improvement compared to D-MP, the column reveals that the difference is indeed significant. For

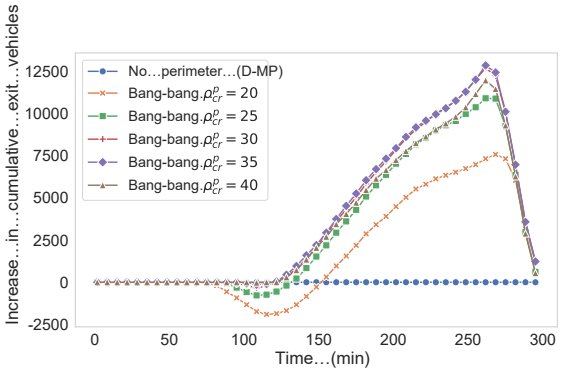

(a) Uniform demand

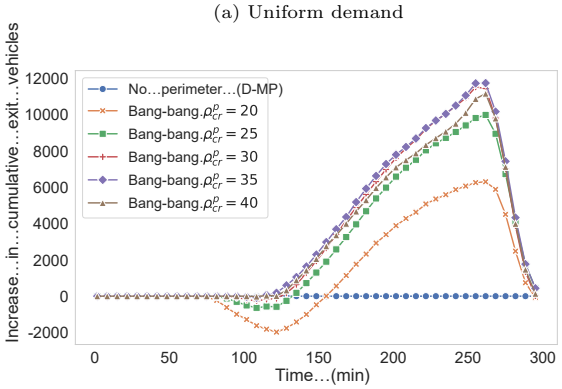

(b) Demand with low imbalance

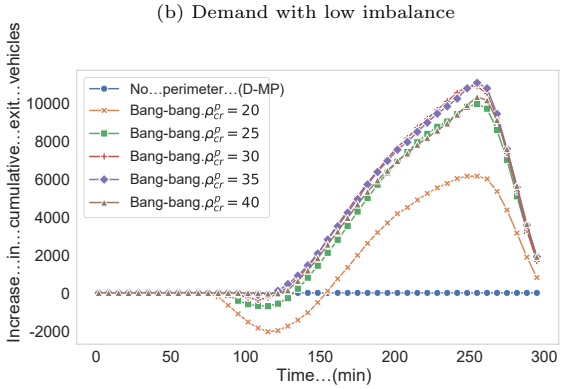

(c) Demand with high imbalance

Figure 7: Impact of ρ_{cr}^{p} on the exit rate under bang-bang control.

example, for the non-uniform demand with high level of imbalance, the largest gap between $\xi = 4$ and $\xi = 5$ is approximately 700 veh around $t = 250$ min. As mentioned before, a larger ξ value imposes a more restrictive control for the inbound movements. When ξ is small, the basic N-MP cannot block enough vehicles to mitigate the congestion in the protected region effectively. At a certain point, the basic N-MP reaches its best performance, and keeping increasing ξ leads to a reduction in the efficiency. Therefore, in general, for all three scenarios, the improvement of the basic N-MP first increases and then decreases with the increase in ξ. The values generating the highest increase in the cumulative exit vehicles are $\xi = 9$, $\xi = 6$ and $\xi = 5$ for the uniform demand, non-uniform demand with low imbalance and non-uniform demand with high imbalance, respectively.

The reductions in travel time, shown in Table 2, are used to quantify the overall improvement from the

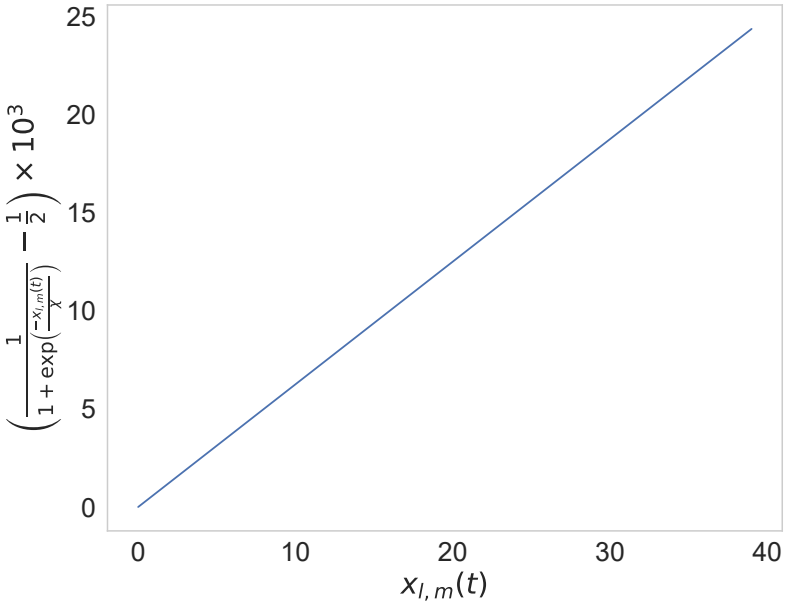

Figure 8: Modified sigmoid function.

basic N-MP. The travel time reduction is relatively stable with the change in ξ. For all cases, the basic N-MP can save the travel time for each vehicle by more than 11 minutes, which is equivalent to a reduction of 20,751 veh-hr in the total travel time.

Table 2: Travel time reduction from the basic N-MP (min/veh)

Demand Scenario	$\xi = 4$	$\xi = 5$	$\xi = 6$	$\xi = 7$	$\xi = 8$	$\xi = 9$	$\xi = 10$
Uniform	-	-	12.46	12.63	12.67	12.89	12.81
Non-uniform low imbalance	11.36	11.31	11.32	11.29	11.32	-	-
Non-uniform high imbalance	11.52	12.00	11.67	11.83	12.22	-	-

3.4.1. Comparison between basic N-MP, bang-bang and FC

For FC, we tested five integral gains: $k_I \in \{0.2, 0.4, 0.6, 0.8, 1\}$. Figure 10 shows the comparisons of the results between the basic N-MP and the baseline models. For the purpose of visualization, we use the cumulative exit vehicles from bang-bang control as the baseline in this figure. For simplicity, only the results from the K_I (for FC) generating the best performance under each scenario are shown.

Figure 10 reveals that the basic N-MP can improve the performance significantly under all demand scenarios compared to the bang-bang control. Although the bang-bang control is theoretically optimal for perimeter control problem (Daganzo, 2007), it does not consider the impact of queue accumulation at the periphery of the protected region on the traffic operations, which can weaken the efficiency in reality. Figure 11 shows the evolution of density inside and outside the protected region for D-MP, the basic N-MP and bang-bang control under the uniform demand. Compared to D-MP (blue), bang-bang (orange) control and the basic N-MP (green) can maintain the density in the protected region around the critical value 35 veh/ln-km. Although the ρ^p from the basic N-MP is slightly higher than the bang-bang control, the average density outside the protected region from the basic N-MP is lower. This lowered density creates a higher

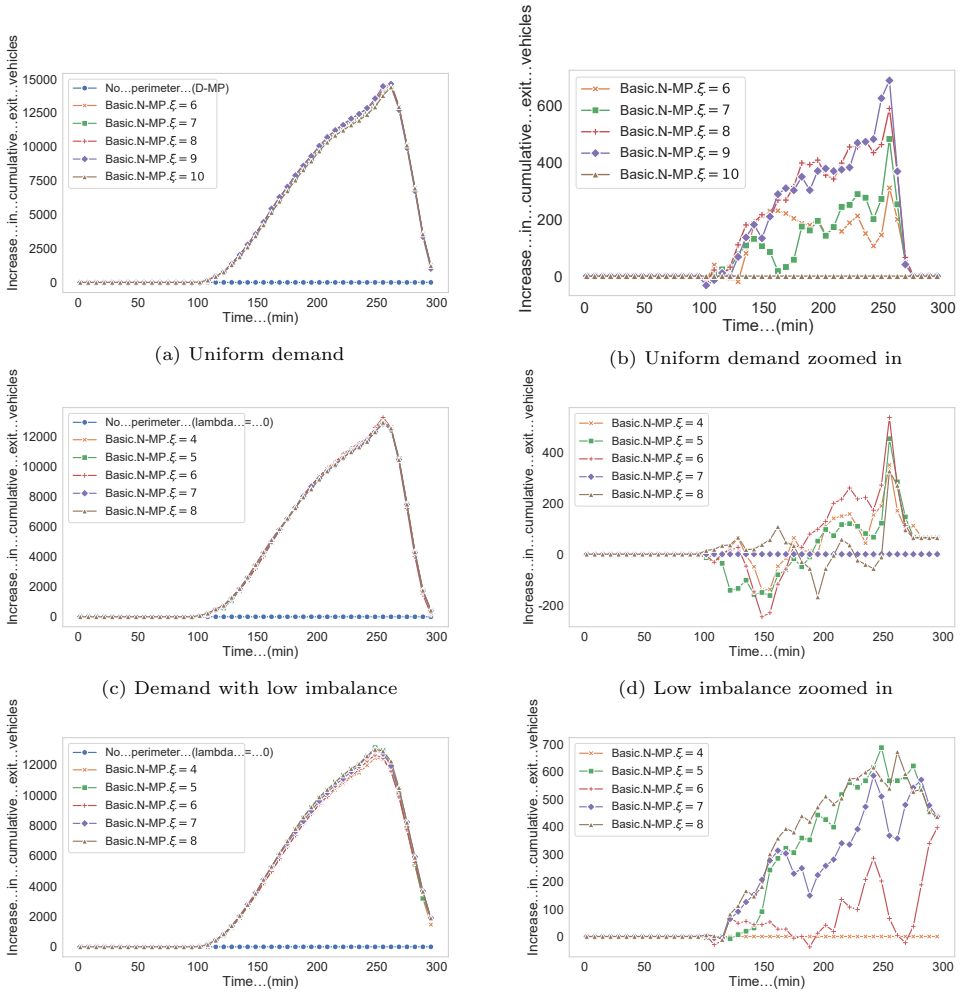

(a) Uniform demand

(b) Uniform demand zoomed in

(c) Demand with low imbalance

(d) Low imbalance zoomed in

(e) Demand with high imbalance

(f) High imbalance zoomed in

Figure 9: Impact of ξ on the efficiency of N-MP.

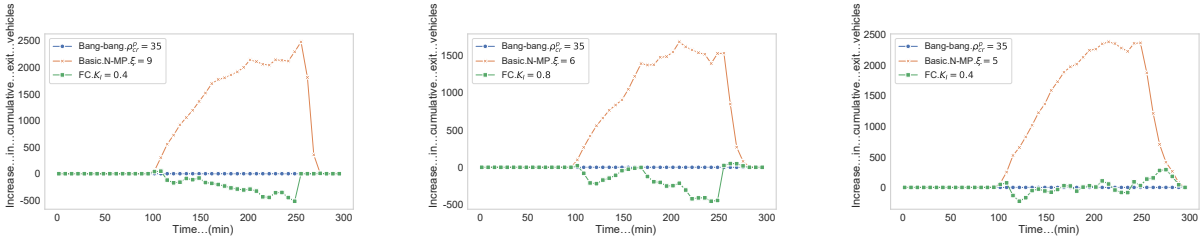

(a) Uniform demand

(b) Low imbalance

(c) High imbalance

Figure 10: Comparison of control performance.

rate for vehicles entering the protected region from the outside region. As a result, it improves the overall efficiency.

Contrary to the findings in (Keyvan-Ekbatani et al., 2012), bang-bang control outperforms FC under all scenarios. One important reason for this discrepancy is that the simulation is time step based with a step size equal to 10 s while the algorithm proposed in (Keyvan-Ekbatani et al., 2012) is cycle-based. The cycle length is generally longer than the time step, so blocking the inbound movements for a cycle could lead to

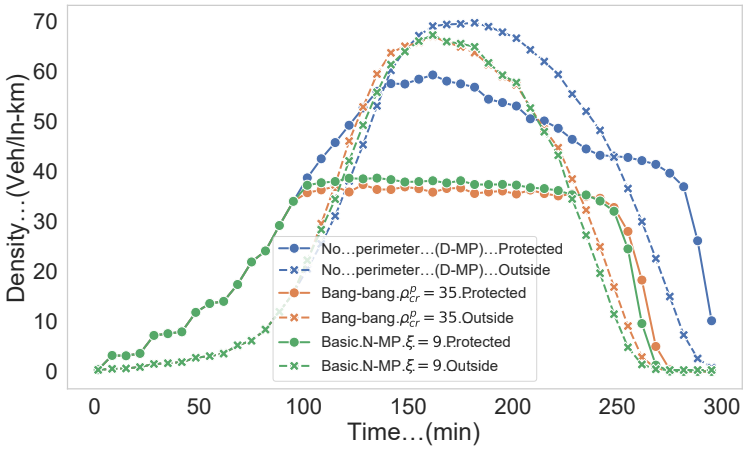

Figure 11: Density evolution under uniform demand.

needless delay if the average density of the protected region drops below the critical value during the middle of the cycle. Therefore, under the cycle-based setting, this algorithm can improve the efficiency compared to bang-bang control. However, under the time step-based traffic operation, the bang-bang control adjusts the signal timing more rapidly, and the restriction will be removed almost immediately once $\rho^p(t) \leq \rho_{cr}^p$, which avoids the drawback existing in the cycle-based setting. On the contrary, FC becomes more insensitive to the traffic states under this situation since it adjusts the signal timing less frequently.

3.4.2. Comparison between clustered N-MP and the basic N-MP

The previous section demonstrates that the basic N-MP algorithm can outperform D-MP and the two baseline PC algorithms. We now compare the performance of the basic N-MP and clustered N-MP. Four cluster orders ($i \in \{1, 2, 3, 4\}$) are tested for each demand scenario. For each order i, the same ten integers for ξ from the basic N-MP are tested. Figure 12 shows the comparison between the basic N-MP and the clustered N-MP. For the purpose of visualization, the basic N-MP is used as the baseline, and only the results from the best ξ are included for each cluster order.

Figure 12b and Figure 12c reveal that the clustered N-MP can further improve the network efficiency for the non-uniform demand scenarios; in fact, all tested cluster orders generate higher vehicle exit rate than the basic N-MP. These advantages result from the balance between the level of congestion in the clusters and the level of inflow restriction at the associated perimeter intersections. Figure 13 shows the average density of clusters associated with perimeter intersections in each demand region, under the control of clustered N-MP with $i = 2, \xi = 1$ for the time period when $\rho^p(t) > \rho_{cr}^p$ for the highly imbalanced demand scenario. The plot clearly shows that the density observed in clusters near the high-demand region is larger.

Furthermore, as described in Section 3.1, all perimeter intersections have four phases and three inbound movement. Each of the inbound movements is served by an unique phase, and there is one phase that does not serve any inbound movements. In order to compare the phase selection mechanism between the basic N-MP and clustered N-MP, when $\rho^p(t) > \rho_{cr}^p$, the activated phase associated with the queue length of the corresponding inbound movements at all perimeter intersections are obtained. Figure 14 shows the frequency for the activated phase associated with this length in both demand regions. We use dark and light colors to indicate the results from the clustered N-MP and the basic N-MP, respectively. It is expected that the clustered N-MP imposes more restricted control for the perimeter intersections adjacent to the high demand region since their clusters are more congested than the low demand region. The first group in Figure 14 shows that, from the clustered N-MP, the perimeter intersections in the high demand region, indicated by the dark orange bar, activate the phase without serving inflows, which is equivalent to block all inbound

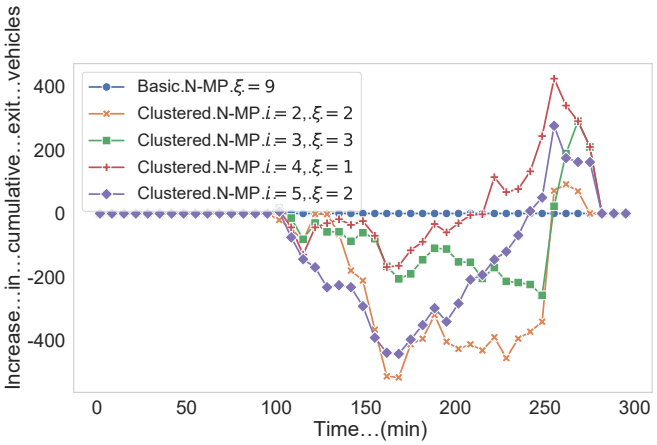

(a) Uniform demand

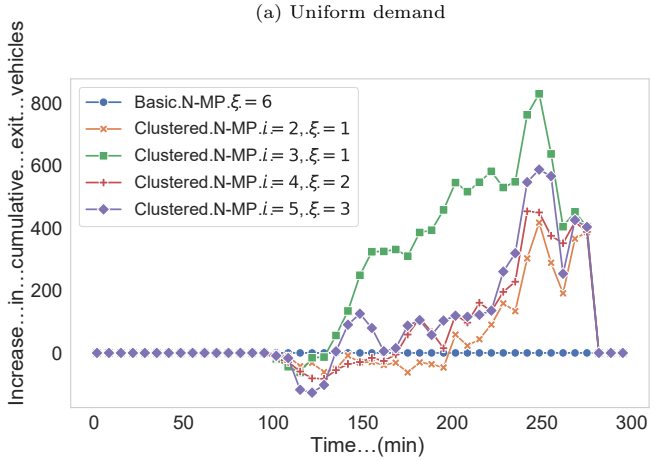

(b) Demand with low imbalance

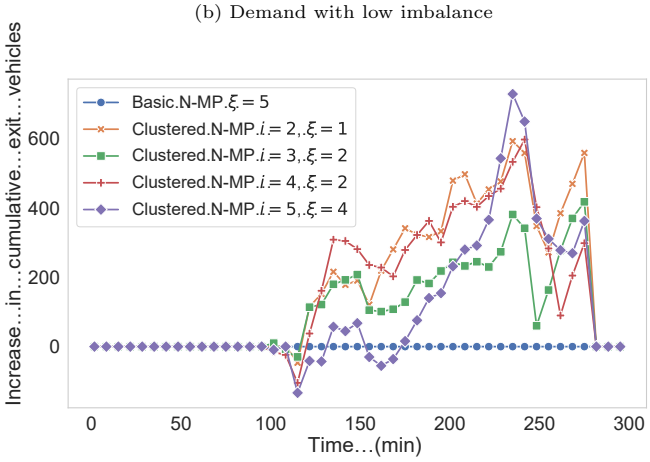

(c) Demand with high imbalance

Figure 12: Comparison of control performance.

vehicles, more often than the lower demand region, indicated by the dark blue bar. On the contrary, as shown by the fourth group, the perimeter intersections in the low demand region activates the phase serving the inbound movements with the longest queue more often than the high demand region. However, this phenomenon is less significant from the basic N-MP.

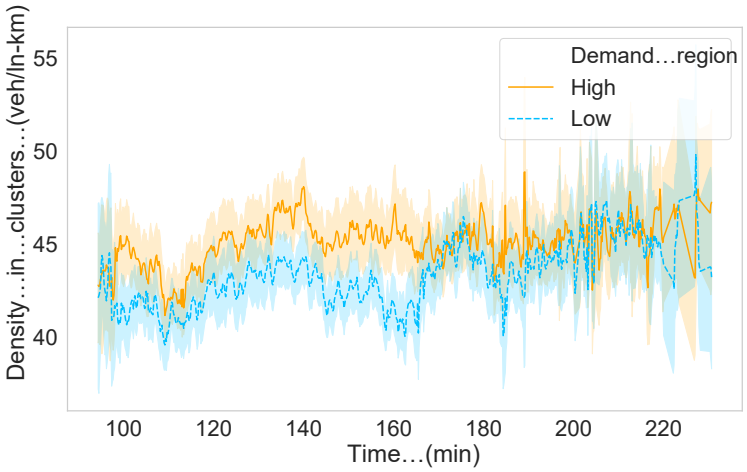

Figure 13: Comparison of density in clusters between two demand regions.

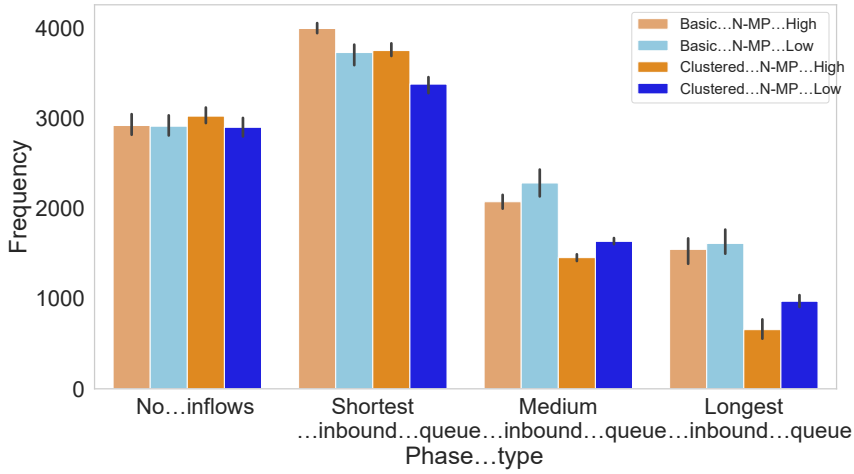

Figure 14: Comparison of phase selection between the basic N-MP and clustered N-MP.

This feature of the clustered N-MP benefits the network efficiency in two ways: first, compared to the basic N-MP, it reduces the unnecessary delays around the less congested region; second, it helps homogenize the network, which contributes the overall mobility when the network is congested. In line with our expectation, these advantages are mitigated when the demand is uniform. As shown in Figure 12a, all cluster orders, except for $i = 4$, generate lower network efficiency compared to the basic N-MP. Thus, the clustered N-MP provides better results only when demand around the perimeter is inhomogeneous, as would be expected.

3.5. Results in a partially connected environment

The results in the previous section are based on a full knowledge of the traffic state across the network. This requires perfectly accurate sensing, which is not realistic or expected. Thanks to the advancement and increasing deployment of connected vehicles (CVs), traffic states can also be obtained via communication between vehicles and infrastructure. Therefore, it is promising to test the proposed models in a partially connected environment with different penetration rates.

Two types of metrics need to be estimated from the CV information. The first is the local delay employed in the basic N-MP and clustered N-MP. This value is approximated using the delay incurred by CVs from the corresponding movement and time step. The second is the average density $\rho^p(t)$ in the protected region; for this, the method developed in (Gayah and Dixit, 2013) is used. This method assumes the well-defined and reproducible MFD of the protected region is available, as shown in Figure 6. Then, the average speed of CVs in the previous time step is used as an approximation of the average speed of all vehicles. Next, based on the one-to-one relationship between the average speed and average density on MFD, an estimation of $\rho^p(t)$ is obtained.

CVs are randomly generated by the simulation, and four penetration rates, {20%, 40%, 60%, 80%}, are tested. It was found that the penetration rate of 20% is too low to generate acceptable control performance. Under this rate, the network becomes completely congested under all control strategies. Therefore, we do not include this value in the results. In addition, according to the results shown in the previous section, we only compare the bang-bang control, the basic N-MP and clustered N-MP with the optimal parameters.

The results are shown in Figure 15. The baseline in Figure 15 is the result of D-MP in a fully connected environment. The results show the efficiency of all control strategies decreases with the decrease in the penetration rate; however, when the penetration rate is higher than 40%, all models in the partially connected environment outperform the D-MP in a fully connected environment. The basic N-MP and clustered N-MP also outperform the bang-bang under all scenarios. Interestingly, the superiority of the clustered N-MP over the basic N-MP vanishes to some extent. When the penetration rate is as low as 40%, the basic N-MP even dominates the clustered N-MP. This is because that information from the whole protected can produce more accurate estimates of the average density than individual clusters when the penetration rate is low. As a result, the basic N-MP generates higher network efficiency than clustered N-MPs under this situation.

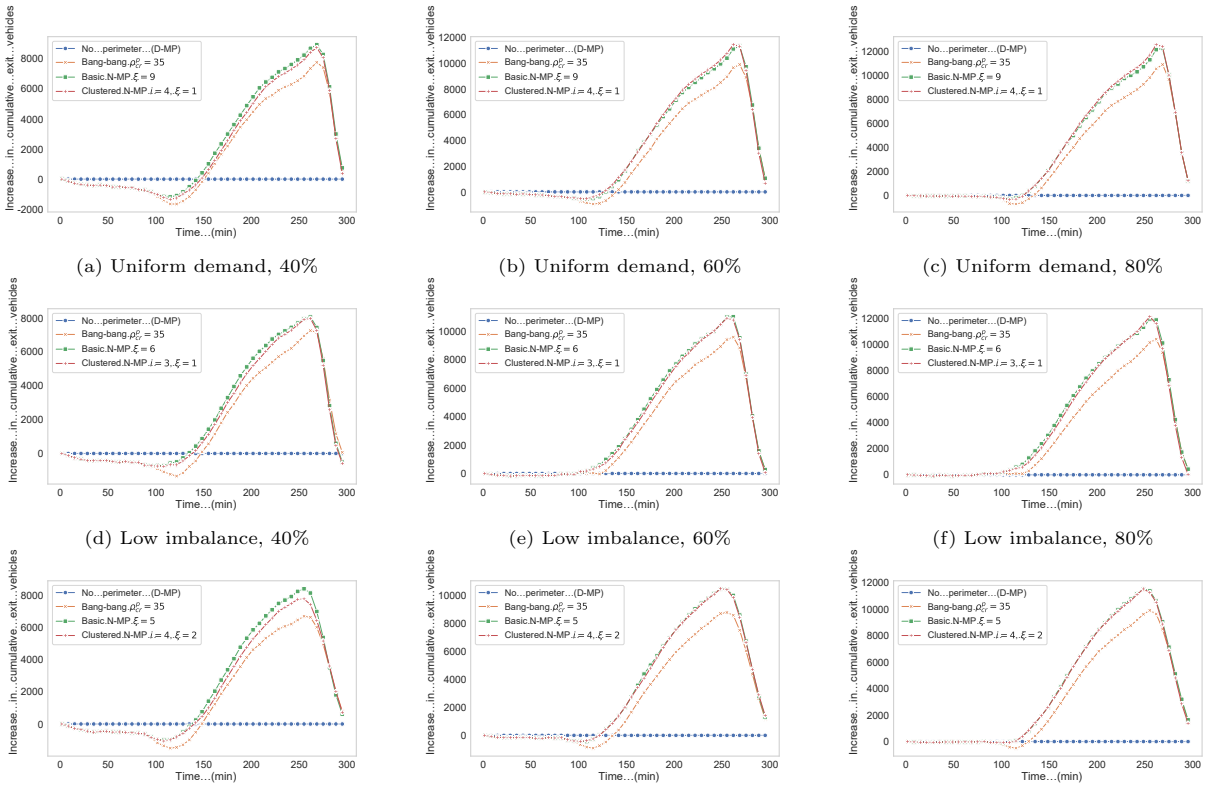

(a) Uniform demand, 40%

(b) Uniform demand, 60%

(c) Uniform demand, 80%

(d) Low imbalance, 40%

(e) Low imbalance, 60%

(f) Low imbalance, 80%

(g) High imbalance, 40%

(h) High imbalance, 60%

(i) High imbalance, 80%

Figure 15: Comparison of control performance in partially connected environment.

4. Concluding Remarks

This paper proposes a novel MP algorithm, N-MP, that incorporates regional perimeter control by considering the traffic state of a protected region in the weight definition of the MP algorithm. The proposed N-MP does not require extra information compared to the basic MP algorithms. Also, it inherits the desirable properties from other MP algorithms, such as the fast computational speed and no need for demand information. More importantly, the N-MP maintains the maximum stability property. We also extend the basic N-MP to a clustered N-MP in which the protected region is divided into clusters based on the distance from the associated inbound movements. Microscopic traffic simulation results show that the proposed models can outperform the bang-bang control and a feedback perimeter control algorithm under various traffic conditions. With a full knowledge of traffic states, the clustered N-MP outperforms the basic N-MP since it considers only the nearby region that can be impacted by the corresponding inbound movements within a short time window. In addition, the performance of the proposed models are tested in partially connected environment. The results shows that the superiority of the proposed models over the bang-bang control remains under these conditions. When the penetration rate is low, the basic N-MP dominates the clustered N-MP due to the higher accuracy of average density estimates within the protected region.

Although the proposed mechanism of incorporating regional perimeter control to an MP-based algorithm is not limited by the used metric for the pressure calculation – e.g., number of vehicles, travel time and travel delay – the parameters in the proposed model are manually tuned and fixed during the whole simulation. A theoretical model that adjusts the parameters according to the real-time traffic conditions is promising. In addition, an extension for the cycle-based MP algorithm is another interesting topic.

Acknowledgement

This research was supported by NSF Grant CMMI-1749200.

References

Alonso, B., Ibeas, Á., Musolino, G., Rindone, C., Vitetta, A., 2019. Effects of traffic control regulation on network macroscopic fundamental diagram: A statistical analysis of real data. Transportation Research Part A: Policy and Practice 126, 136–151.

Daganzo, C.F., 2007. Urban gridlock: Macroscopic modeling and mitigation approaches. Transportation Research Part B: Methodological 41, 49–62.

Daganzo, C.F., Gayah, V.V., Gonzales, E.J., 2011. Macroscopic relations of urban traffic variables: Bifurcations, multivaluedness and instability. Transportation Research Part B: Methodological 45, 278–288.

Dixit, V., Nair, D.J., Chand, S., Levin, M.W., 2020. A simple crowdsourced delay-based traffic signal control. PLoS one 15, e0230598.

Gartner, N.H., 1983. OPAC: A demand-responsive strategy for traffic signal control. 906.

Gayah, V.V., Daganzo, C.F., 2011. Effects of turning maneuvers and route choice on a simple network. Transportation Research Record 2249, 15–19.

Gayah, V.V., Dixit, V.V., 2013. Using mobile probe data and the macroscopic fundamental diagram to estimate network densities: Tests using microsimulation. Transportation research record 2390, 76–86.

Geroliminis, N., Daganzo, C.F., 2008. Existence of urban-scale macroscopic fundamental diagrams: Some experimental findings. Transportation Research Part B: Methodological 42, 759–770.

Godfrey, J., 1969. The mechanism of a road network. Traffic Engineering & Control 8.

Gregoire, J., Qian, X., Frazzoli, E., De La Fortelle, A., Wongpiromsarn, T., 2014. Capacity-aware backpressure traffic signal control. IEEE Transactions on Control of Network Systems 2, 164–173.

Haddad, J., Shraiber, A., 2014. Robust perimeter control design for an urban region. Transportation Research Part B: Methodological 68, 315–332.

Hao, Z., Boel, R., Li, Z., 2018. Model based urban traffic control, part i: Local model and local model predictive controllers. Transportation research part C: emerging technologies 97, 61–81.

Hunt, P., Robertson, D., Bretherton, R., Winton, R., 1981. SCOOT-a traffic responsive method of coordinating signals. Technical Report.

Keyvan-Ekbatani, M., Kouvelas, A., Papamichail, I., Papageorgiou, M., 2012. Exploiting the fundamental diagram of urban networks for feedback-based gating. Transportation Research Part B: Methodological 46, 1393–1403.

Knoop, V.L., De Jong, D., Hoogendoom, S.P., 2014. Influence of road layout on network fundamental diagram. Transportation Research Record 2421, 22–30.

Le, T., Kovács, P., Walton, N., Vu, H.L., Andrew, L.L., Hoogendoorn, S.S., 2015. Decentralized signal control for urban road networks. Transportation Research Part C: Emerging Technologies 58, 431–450.

Levin, M.W., 2023. Max-pressure traffic signal timing: A summary of methodological and experimental results. Journal of Transportation Engineering, Part A: Systems 149, 03123001.

Levin, M.W., Hu, J., Odell, M., 2020. Max-pressure signal control with cyclical phase structure. Transportation Research Part C: Emerging Technologies 120, 102828.

Li, L., Jabari, S.E., 2019. Position weighted backpressure intersection control for urban networks. Transportation Research Part B: Methodological 128, 435–461.

Liu, H., Gayah, V.V., 2022. A novel max pressure algorithm based on traffic delay. Transportation Research Part C: Emerging Technologies 143, 103803.

Liu, H., Gayah, V.V., 2023. Total-delay-based max pressure: A max pressure algorithm considering delay equity. Transportation Research Record , 03611981221147051.

Lowrie, P., 1990. Scats, sydney co-ordinated adaptive traffic system: A traffic responsive method of controlling urban traffic .

Mauro, V., Di Taranto, C., 1990. Utopia. IFAC Proceedings Volumes 23, 245–252.

Mercader, P., Uwayid, W., Haddad, J., 2020. Max-pressure traffic controller based on travel times: An experimental analysis. Transportation Research Part C: Emerging Technologies 110, 275–290.

Mirchandani, P., Head, L., 2001. A real-time traffic signal control system: architecture, algorithms, and analysis. Transportation Research Part C: Emerging Technologies 9, 415–432.

Ni, W., Cassidy, M.J., 2019. Cordon control with spatially-varying metering rates: A reinforcement learning approach. Transportation Research Part C: Emerging Technologies 98, 358–369.

Ortigosa, J., Menendez, M., 2014. Traffic performance on quasi-grid urban structures. Cities 36, 18–27.

Ramezani, M., Haddad, J., Geroliminis, N., 2015. Dynamics of heterogeneity in urban networks: aggregated traffic modeling and hierarchical control. Transportation Research Part B: Methodological 74, 1–19.

Su, Z., Chow, A.H., Fang, C., Liang, E., Zhong, R., 2023. Hierarchical control for stochastic network traffic with reinforcement learning. Transportation Research Part B: Methodological 167, 196–216.

Tassiulas, L., Ephremides, A., 1990. Stability properties of constrained queueing systems and scheduling policies for maximum throughput in multihop radio networks, in: 29th IEEE Conference on Decision and Control, IEEE. pp. 2130–2132.

Tsitsokas, D., Kouvelas, A., Geroliminis, N., 2023. Two-layer adaptive signal control framework for large-scale dynamically-congested networks: Combining efficient max pressure with perimeter control. Transportation Research Part C: Emerging Technologies 152, 104128.

Varaiya, P., 2013. Max pressure control of a network of signalized intersections. Transportation Research Part C: Emerging Technologies 36, 177–195.

Wang, X., Yin, Y., Feng, Y., Liu, H.X., 2022. Learning the max pressure control for urban traffic networks considering the phase switching loss. Transportation Research Part C: Emerging Technologies 140, 103670.

Wu, J., Ghosal, D., Zhang, M., Chuah, C.N., 2017. Delay-based traffic signal control for throughput optimality and fairness at an isolated intersection. IEEE Transactions on Vehicular Technology 67, 896–909.
Xiao, N., Frazzoli, E., Li, Y., Wang, Y., Wang, D., 2014. Pressure releasing policy in traffic signal control with finite queue capacities, in: 53rd IEEE Conference on Decision and Control, IEEE. pp. 6492–6497.
Xu, G., Gayah, V.V., 2023. Non-unimodal and non-concave relationships in the network macroscopic fundamental diagram caused by hierarchical streets. Transportation Research Part B: Methodological 173, 203–227.
Xu, G., Yu, Z., Gayah, V.V., 2020. Analytical method to approximate the impact of turning on the macroscopic fundamental diagram. Transportation research record 2674, 933–947.
Xu, T., Barman, S., Levin, M.W., Chen, R., Li, T., 2022. Integrating public transit signal priority into max-pressure signal control: Methodology and simulation study on a downtown network. Transportation Research Part C: Emerging Technologies 138, 103614.
Zhang, L., Garoni, T.M., de Gier, J., 2013. A comparative study of macroscopic fundamental diagrams of arterial road networks governed by adaptive traffic signal systems. Transportation Research Part B: Methodological 49, 1–23.
Zhang, L., Yuan, Z., Yang, L., Liu, Z., 2020. Recent developments in traffic flow modeling using macroscopic fundamental diagram. Transport reviews 40, 529–550.
Zhou, D., Gayah, V.V., 2021. Model-free perimeter metering control for two-region urban networks using deep reinforcement learning. Transportation Research Part C: Emerging Technologies 124, 102949.
Zhou, D., Gayah, V.V., 2023. Scalable multi-region perimeter metering control for urban networks: A multi-agent deep reinforcement learning approach. Transportation Research Part C: Emerging Technologies 148, 104033.